LM-06K055
May 22, 2006

Generation of Tones Due to Flow past a Deep Cavity: Effect of Streamwise Length

Y Yang, D Rockwell, K Lai-Fook Cody, M Pollack

GENERATION OF TONES DUE TO FLOW PAST A DEEP CAVITY: EFFECT OF STREAMWISE LENGTH

Y. Yang[*] D. Rockwell[*]
K. Lai-Fook Cody[-1-] M. Pollack[-1-]

[*] Lehigh University, Bethlehem, PA
[-1-] Lockheed-Martin, Schenectady, NY

ABSTRACT

Shear flow past a deep cavity can generate self-sustained oscillations, including locked-on flow tones due to coupling between the inherent instability of the separated shear layer and an acoustic mode of the cavity resonator. This investigation focuses on the pressure amplitude response within a deep cavity, as a function of the streamwise length of the cavity opening; for each length, the pressure amplitude response is characterized over a wide range of inflow velocity.

Criteria for locked-on flow tones are assessed; they include: a measure of the strength of lock-on, *SoL*; and the quality factor *Q*. All self-excited oscillations are assessed using both of these criteria, in order to interpret dimensionless forms of the fluctuation pressure amplitude.

The pressure amplitude response of the cavity involves several successive regimes, due to variations of streamwise length L of the cavity opening. These regimes are defined in relation to L/θ, where θ is the momentum thickness of the inflow boundary layer. Below a minimum value of L/θ, flow tones cannot be generated. Furthermore, these regimes are defined in terms of the possible hydrodynamic modes (stages) of the unsteady shear layer and the acoustic modes of the deep cavity.

1. INTRODUCTION

Flow-acoustic coupling, which involves coupling between a hydrodynamic mode (stage) of a separated shear layer and an acoustic mode of an adjacent resonator, occurs in a broad range of engineering applications. A brief overview of investigations, which are related to those of the present study, is given in the following.

1.1 FLOW-ACOUSTIC COUPLING IN ENGINEERING CONFIGURATIONS

The instability of a separated-shear layer serves as a hydrodynamic source, which can couple with one or more of the modes of an adjacent resonator. This concept, which is present in many different flow configurations, is reviewed by Rockwell and Naudascher (1978, 1979), Rockwell (1983, 1998), Blake (1986), and Rockwell et al. (2003). Previous investigations of flow past cavity configurations indicate that flow tones are attainable not only for rectangular cavities, but also for three-dimensional (nonrectangular) cavity geometries.

If one considers a broader range of flow configurations, extending beyond a single cavity, it is evident that pronounced flow tones can occur. These configurations include jet excitation of a long (closed) organ pipe (Cremer and Ising, 1967; Fletcher, 1974, 1976, 1979), jet-sequential orifice plates (Howe, 1975, 1980; Flatau and Van Moorhem, 1990; Hourigan et al., 1990), wake from a plate in a test section (Parker, 1966; Cumpsty and Whitehead, 1971; Stoneman et al., 1988), shear layer-cavity resonator (DeMetz and Farabee, 1977; Elder, 1978; Nelson et al., 1981, 1983), and cavity shear layer-long pipeline (Pfizenmaier, 1973; Schachenmann and Rockwell, 1980; Rockwell and Schachenmann, 1982a, 1982b; Rockwell and Karadogan, 1982, 1983; Davies, 1981, 1996a, 1996b; Rockwell et al., 2003; Geveci et al., 2003; Oshkai et al., 2004). The configuration of a cavity shear layer-side branch (deep cavity) is not addressed in the foregoing. This configuration, which is of primary interest in the present study, is described in detail in the following sections.

1.2 FLOW-ACOUSTIC COUPLING IN SINGLE SIDE BRANCHES

Of particular practical importance is the occurrence of flow-acoustic coupling that involves resonance of the side branch of the duct, which may, in some cases, couple with a resonant mode of the main duct. Ingard and Singhal (1976) characterize coupling

phenomena involving modes of the side branch and the main duct. Bruggeman (1987) addressed several basic characteristics of a side branch resonator in a main pipe (duct). The acoustic plexus in both the side branch and the main pipe is described, as well as the radiation condition at the exhaust of the pipe, which had an influence on the maximum attainable pressure amplitude at the dead end of the side branch resonator. Many of these aspects are also described by Bruggeman et al. (1989, 1991). Ziada and Bühlmann (1992) address the case of a single side branch in which a main duct is extended to a long pipe with an absorption silencer, thereby limiting the pressure amplitude to very low values. Ziada and Bühlmann (1992) summarize the consequences of radiation, friction and heat losses along the amplitude of the pressure fluctuation at the dead end of the side branch, by in-depth consideration of the data of Jungowski et al. (1989), which indicate the importance of the ratio of the diameter of the side branch to the diameter of the main duct on the maximum attainable pressure amplitude at the end of the side branch. Hofmans (1998) provides quasi-steady and numerical models of a single side branch connected to a main duct, accounting for the direction of mean flow and the acoustic flux of the side branch to the main duct. This numerical simulation provided insight into the amplitude of the pressure fluctuation at the dead end of the side branch, in relation to reflection conditions at the end of the main duct.

Horizontal to the foregoing investigations has involved a side branch (deep cavity-main duct) configuration. Dequand (2001) considers the case of an isolated deep cavity exposed to the free atmosphere. Very strong flow tones were attainable for this configuration. Geometric changes of the cavity mouth (opening) were related to amplitude of pulsation at the dead end of the deep cavity.

1.3 FLOW-ACOUSTIC COUPLING IN COAXIAL AND TANDEM SIDE BRANCHES

A coaxial side branch system involves two side branches located in line with each other, on opposite sides of the main duct. Ziada and Bühlmann (1992) and Kriesels et al. (1995) demonstrate that large amplitudes of the fluctuating pressure at the dead ends of the side branches can be attained. It is generally accepted that radiation damping from each side branch is minimized for this coaxial configuration, which enhances the maximum attainable amplitude.

A tandem side branch configuration involves two successive side branches on the same side of the main duct. Bruggemann (1987), as well as Bruggemann et al. (1989, 1991), show that large pressure amplitudes can be attained at the dead end of the side branch, provided the spacing between the branches allows existence of a favorable phase relationship between them. This configuration was further investigated by Ziada and Bühlmann (1992).

1.4 UNRESOLVED ISSUES

On the basis of the state-of-the-art side branch resonators described in the foregoing, it is possible to define a number of key issues that require clarification. They are briefly outlined in the following. In doing so, the terminology of an isolated deep cavity is intended to represent a deep cavity in absence of coupling effects with a main duct.

(a) The onset of a flow tone in an isolated deep cavity has not been addressed in terms of the streamwise length of the cavity opening in relation to the boundary layer thickness of the inflow. When all other parameters in the flow and acoustic system are held constant, it should be possible to find a critical value of dimensionless streamwise length at which the onset of the flow tone occurs.

(b) As the dimensionless length of the opening of the deep cavity is successively increased beyond the minimum value defined in (a), certain hydrodynamic modes (stages) of the shear layer along the cavity opening and detectable acoustic modes of the deep cavity will become distinctly defined. Furthermore, for certain of these combinations, the resonant coupling between them will be sufficient such that a coupled flow tone is generated. These phenomena have not been characterized. It should be possible to define regimes of response with increasing values of dimensionless streamwise cavity length, which incorporate detection of, and coupling between, definable hydrodynamic modes (stages) and acoustic modes.

(c) For a given value of dimensionless streamwise length of the cavity, a minimum critical velocity, for which the onset of a flow tone first occurs, should be defined. At values of velocity larger than this critical value, the manner in which resonant coupling occurs between the hydrodynamic modes (stages) and acoustic modes should be defined in detail.

(d) The criteria for defining the onset of a flow tone needs to be assessed and compared with each other. Two possibilities include a strength of lock-on *SoL* criterion, which involves the amplitude of the pressure fluctuation at the dead end of the cavity, in excess of a reference (background) amplitude, and a quality Q factor of the spectral peak of the pressure fluctuation at the dead end of the cavity.

(e) The role of linear, inviscid stability theory in providing guidance for interpretation of the effective amplitude of the pressure fluctuation of the dead end of the cavity, for variations in dimensionless streamwise cavity length, has yet to be assessed.

The present investigation aims to address the foregoing issues.

2. EXPERIMENTAL SYSTEM AND TECHNIQUES

2.1 OVERVIEW OF EXPERIMENTAL SYSTEM

All components of the experimental system, both upstream of, and including the main test section, were designed and fabricated in the Fluid Mechanics Laboratories at Lehigh University. Two principal subsystems comprise the overall experimental system. The first subsystem is the air conditioning and supply system, and the second is the actual inlet duct-deep cavity system. The first subsystem is located in a separate room, which is isolated from the room containing the inlet duct-deep cavity system. This approach allows isolation of undesirable mechanical vibrations and acoustic effects associated with the air compressor system.

A compressor maintains air at a pressure of 552-689 KPa (80-100 psig) in a plenum, which is stored in a compressed air plenum. At the outlet of the plenum, an air dryer arrangement allows separation of residual water from the air, and a filter system extracts foreign particles. The dried and filtered air is transmitted through the isolation wall into the room that houses the main experimental facility, i.e., the main duct – deep cavity arrangement with its associated plenum.

An overview of the main duct – deep cavity facility is provided in Figure 1. It consists of an arrangement of valves, an inlet plenum, three-dimensional nozzle, which precedes a rectangular cross-section main duct that is terminated by the deep cavity.

The system of valves and regulators shown at the left of Figure 1 is made up of a throughflow and a bypass arrangement. This dual path for the incoming air allows a wide range of mass flow rates. The flow from the valve-regulator systems passes through a long flexible hose, which has an inside diameter of 25.4 mm and a total length of 5 m. It was found that this longer hose very effectively attenuated high frequency disturbances generated by the valve-regulator system. The downstream end of this flexible hose was connected to the inflow port of the inlet plenum. Within the plenum, the air flow expanded, passed through a flow conditioner (honeycomb), then was accelerated in a three-dimensional nozzle, which, in turn, fed into the main duct.

The entire inlet plenum-nozzle-main duct system was supported by means of rigid struts, which were connected to an optical bench.

In the following, the components of the main duct-deep cavity system are described in detail.

2.2 MAIN TEST SECTION

Inlet plenum. The inlet plenum of the main duct-deep cavity system, as shown in Figure 1, was constructed entirely of Plexiglas. A honeycomb system located within the plenum attenuates flow disturbances. The interior surface of the plenum is lined with acoustic damping foam, in order to attenuate the local acoustic resonances.

Three-dimensional nozzle. A three-dimensional nozzle was connected to the exit of the plenum. It was manufactured using a rapid prototyping technique, and designed to optimize the acceleration of flow from a relatively low velocity in the plenum to a high velocity at the inlet of the main duct. The internal dimensions of the exit of the three-dimensional nozzle matched the dimensions of the inlet of the main duct. These dimensions are given in the next section.

Main duct subsystem. The main duct, which was attached to the exit of the three-dimensional nozzle described in the preceding subsection, is shown in Figure 1. The internal dimensions of this duct were 38.1 mm × 25.4 mm. The downstream end of the duct exhausted into the open atmosphere. Moreover, the duct was bounded on three sides over its entire length of 570 mm, except for one open side, which is evident in the close-up of Figure 1. This open side allowed decoupling of the flow through the main duct and the

resonance of the deep cavity. Other features of the main duct arrangement include a boundary layer trip, which involved a rectangular bar of streamwise length 5 mm and height 1.5 mm, in order to promote transition of the boundary layer emanating from the three-dimensional nozzle. A static pressure tap was located immediately downstream of the boundary layer trip, in order to provide a reference steady pressure for measurement of flow rate through the main duct.

Near the downstream end of the duct, a vortex generator and sawtooth plate were located at the separation lip shown in the close-up of Figure 1. The purpose of this arrangement was to attenuate the process of vortex formation from the lip of the duct end. The effectiveness of this arrangement was verified by spectra of hotwire measurements, as well as detailed quantitative images of the flow structure. These approaches show that no coherent vortex formation occurred downstream of this edge of the duct. In essence, this arrangement was effective for two primary reasons: the vortex generator yielded patterns of streamwise vorticity and, furthermore, the sawtooth arrangement prevented the effective conversion of the disturbances from the radiated acoustic wave front to spanwise coherent vorticity concentrations at the lip. The vortex generator had protrusions of height 5 mm; these triangular protrusions were at an angle of 45º with respect to the incident free stream. Moreover, they had a wavelength of 8 mm along the span of the duct. The sawtooth extension had a peak to trough distance of 5 mm and a spanwise wavelength of 8 mm. The crests of the sawtooth arrangement protruded a distance of 7 mm from the lip of the main duct.

The locations for three flush-bounded pressure transducers are indicated in the plan view of Figure 1. These pressure transducers were employed to monitor the amplitude and frequency of organized spectral components within the main duct, in order to ensure that negligible coupling occurred between the main duct and the deep cavity.

Deep cavity arrangement. Details of the deep cavity are shown in the plan view and the close-up of Figure 1. The cavity duct is made of an aluminum tube, which is of a rectangular cross-section, with wall thickness of 3.2 mm. The total depth of the cavity is designated as L_C. This total depth involves the sum of the actual cavity duct and a Plexiglas spacer, along with the thickness of the main duct. For present investigation, the total depth

is fixed at L_C = 482.6 mm. The length L of the cavity opening had values of 25.4 mm, 50.8 mm and 76.2 mm. Smaller values of L were attained by fixing aluminum plate spacers within the deep cavity rigidly.

The end of the deep cavity was terminated by an aluminum endplate having a thickness of 12.7 mm. It housed a PCB pressure transducer, which will be described in a following subsection.

The naturally-generated boundary layer was characterized at a location immediately upstream of the leading edge of the cavity opening, i.e., at a distance of 8 mm upstream of the leading edge of the cavity. This location corresponds to the profile of time-averaged streamwise velocity in the close-up of Figure 1. The acquisition of such velocity profiles at different values of mean inflow velocity U is accomplished using a total pressure probe and a static wall tap (not shown). Then the values of momentum thickness θ are determined from these profiles in relation to U. Experimental results show that variation of momentum thickness θ follows the one-fifth law of the turbulent boundary layer very well. Specifically, $\theta = 1.154\ U^{-1/5}$, where θ is in mm and inflow velocity U is in m/s. Therefore, this analytical expression is employed throughout the present investigation to evaluate the inflow boundary layer momentum thickness θ.

Main duct – deep cavity system: ***decoupling of acoustic characteristics.*** An essential aspect of the design of the main duct and the deep cavity described in the preceding subsection is that they have different resonant frequencies, in order to minimize possible coupling between these two major components. A central consideration is that the resonant frequencies of the main duct are not coincident with those of the deep cavity. Thus in the design phase, the depths L_C were selected such that the resonant frequencies of the deep cavity were well removed from a given resonant frequency of the main duct.

2.3 ACQUISITION AND PROCESSING OF PRESSURE DATA

Pressure transducers. High-sensitivity, flush mounted pressure transducers were employed; they had a nominal sensitivity of 1727 mv/psi. The outputs from the transducers were connected to a multi-channel signal conditioner. This multi-channel conditioner allowed independent adjustment of the gains of the pressure transducer signals. Generally speaking, however, it was possible to employ the same value of gain for all pressure

measurements. This gain adjustment is important in order to meet the required voltage input levels of the A/D (analog/digital) board.

Acquisition of pressure signals. The conditioned pressure signals were transmitted to ports on a data acquisition with 12-bit resolution. This board, when operating in the single channel acquisition mode, can sample at the rate of 250 *KS*/s, in which $K = 10^3$ and *S* is the number of samples. In the present scenario, a total of eight channels (four connected to pressure transducers and four empty) were employed, so the effective sampling rate is reduced by a factor of eight, i.e., it takes on a value of 31 *KS*/s per channel. In essence, there are two considerations to determine whether this sampling rate is adequate. First of all, for characterization of pressure in the frequency domain, the sampling rate should be at least twice the maximum frequency of interest. For representations in the time domain, a minimum of five samples per cycle is required, but a minimum of ten samples per cycle is desirable. Considering these requirements together, the acquisition system should have a sampling rate at least ten times as high as the maximum typical frequency of interest in the present investigation, which corresponds approximately to 1.7×10^4 Hz. This requirement is approximately a factor of two lower than the acquisition rate of 31 *KS*/s per channel. It is also important to realize that this type of board basically consists of one A/D (analog digital) converter, and the acquisition of eight pressure signals is accomplished using a multiplexing technique. The scan interval is defined as the time required to go from a recorded point corresponding to pressure transducer No. 1, through the sequence of the other transducers, and return to the channel of transducer No.1. This scan interval is basically the inverse of the maximum data acquisition rate per channel is $1/(31.25 \times 10^3)$, which corresponds approximately to 32 microseconds.

Processing of pressure signals. LabView software was used to process the pressure transducer signals. The major parameters for spectral analysis using the Fast Fourier Transform (FFT) must be properly defined so that adequate resolution in the frequency domain is accomplished, while at the same time minimizing the amount of collected data. In order to determine which values of each parameter were adequate, a series of averaging tests were performed using broadband noise input. For a given set of parameters, the

number of averaged files was varied to determine the minimum number of files and, hence, the minimum number of data samples needed to properly represent the system response.

The parameters were: (i) the number of samples acquired per data set; (ii) the sampling rate; and (iii) the number of data sets employed to obtain an average. The sampling rate must be twice as high as the maximum frequency of interest. Therefore, the necessary sampling rate varied directly with the maximum frequency of interest for each experiment. The value of the frequency resolution (Δf) is equal to the sampling rate (f_s) divided by the number of samples per data set (n_s). Once the sampling rate was determined for each experiment, the number of samples was calculated according to $n_s = f_s/\Delta f$.

In order to determine the value for Δf, another set of averaging experiments was performed. Values of Δf were varied. These tests showed that Δf = 0.5 Hz adequately characterized the system response, while providing acceptable frequency resolution at both the low and high ends of the frequency range of interest to these experiments. At the lowest and highest frequencies of interest, approximately 42 and 1,665 Hz, $\Delta f/f$ has its maximum and minimum values of 0.012 and 0.0003 respectively.

During acquisition of final experimental data, the sampling rate was set to 4,096 samples per second, which resulted in a Nyquist frequency of 2,048 Hz, well above the maximum frequency component of interest for this research, which was approximately 1,700 Hz. The number of samples per data set (n_s) was then specified, while maintaining Δf = 0.5 Hz, resulting in 2^{13} = 8,192 samples per data set. Each of the spectra represented herein was obtained by averaging a total of 40 data sets. Furthermore, the convergence of the calculated spectra as a function of the number of averaged spectra was undertaken using the band-limited white noise technique of loudspeaker excitation. This process was employed for a number of selected resonant modes of a deep cavity. Generally speaking, as few as ten averages yielded a peak spectral amplitude that was indistinguishable from the value determined from a larger number of averages, up to a total of one hundred averages, within an uncertainty of 5%.

3 ONSET AND DEVELOPMENT OF FLOW TONES: PRESSURE RESPONSE CHARACTERISTICS

To determine the effect of streamwise length of the cavity opening on the generation of flow tones, a series of cavities having the same depth but various streamwise lengths were employed during experiments. The cavity depths are fixed at a moderate value of L_C = 482.6 mm, which, with the end correction, corresponds to an effective cavity depth of L_{eff} = 501.7 mm. The cavity lengths vary over the range from L = 12.7 mm to 76.2 mm.

3.1 METHODS OF PRESENTATION OF DATA

In general, the occurrence of flow tones is directly related to flow-acoustic coupling. Figure 2 demonstrates basic concepts and designations of such flow phenomenon. From acoustic perspective, to excite an acoustic resonance in a deep cavity, the incident and reflected waves must form a standing wave along the cavity, and this standing wave must have a pressure node at the open end and a pressure anti-node at the dead end. As shown in Figure 2a, a quarter wave satisfies these conditions, and thus represents an acoustic resonant mode, namely *a1* mode. Similarly, a 3-quarter wave (*a3*) works, a 5-quarter wave (*a5*) works, and so on.

Then hydrodynamically, as shown in Figures 2b and 2c, when shear flow approaches the cavity mouth, under certain conditions, depending on the inflow velocity U and the streamwise length L of the cavity, one wavelength of unsteady shear layer fluctuation may fit in the cavity mouth. If the frequency of this unsteady fluctuation coincides with one of those acoustic modes, flow tone occurs. In this case, one wavelength of the shear layer fluctuation is related to the development of one large scale vortex along the cavity mouth, and it is called the first hydrodynamic mode, namely *h1* mode. Accordingly, subject to proper conditions, the second (*h2*), or even the third (*h3*) hydrodynamic mode may also occur.

To present and characterize flow tone behavior, for each cavity at a given inflow velocity, a time trace of pressure response at the dead end of the cavity was recorded. Then the result was presented in the frequency domain as amplitude spectrum. Following the same procedure, by varying inflow velocity sequentially, a total of approximately 69 spectra were acquired, with each spectrum corresponding to a specified inflow velocity. It is insightful to employ a unified and comprehensive means of presentation and interpretation of families of these spectra. Use of a color-coded, isometric view, as given in

the top plot of Figure 3c (to be discussed in Section 3.2), was constructed for this purpose. In this type of plots, the magnitudes of the pressure are color-coded. This allows inspection of variations of color in two-dimensional space, in turn yielding an overview of the conditions corresponding to generation of relatively high-pressure amplitudes. The emphasis of the present investigation is on characterization for the onset of flow tones; therefore, the largest variations of color level occur at lower values of pressure amplitude. It is important to recognize that, when a threshold value of amplitude is exceeded, the same color (white) magnitude is maintained for all higher values of amplitude. It is therefore not possible to determine, in certain cases, the maximum amplitude of the pressure spectra based on three-dimensional color plots.

A general pattern of aforementioned isometric color plots, such as the one shown in the top plot of Figure 3c, shows some crests along some roughly fixed frequencies. These crests are related to acoustic resonance along the deep cavity, with each of them representing an acoustic *a* mode. On each crest there are also some high amplitude peaks. These peaks are caused by interaction, or coupling, of acoustic resonance and shear layer fluctuation; with each of them representing a flow tone.

In addition to the three-dimensional color plot, corresponding plan view is also provided. This view allows straightforward designation of the hydrodynamic *h* and acoustic *a* mode of each of the peaks, as well as linear fits through these peaks in order to determine dimensionless values of frequency, e.g., Strouhal number. These types of designations are, for example, evident in the bottom plot of Figure 3c.

3.2 EFFECT OF LENGTH OF CAVITY OPENING AT MODERATE CAVITY DEPTH

The effect of variations of the length L of the cavity opening, at a constant value of cavity depth, L_C = 482.6 mm, are given in Figures 3a through 3e. This series of experiments allows identification of minimum value of L at which flow tones can be generated and, furthermore, provide characterization of the flow tones at relatively large values of length L of the cavity opening. That is, nearly all previous investigations of deep cavities as portions of T-junctions have employed values of length L that are the same value as the transverse width of the inflow duct.

In the descriptions that follow, the *Q*-factor is employed as an index of the degree of lock-on. The *Q* factor is defined as $Q = f_0/(f_2 - f_1)$, in which f_0 is the frequency of the tone, and f_1 and f_2 are the frequencies at the half-power points of the spectral peak.

For the smallest value of length *L* of the cavity opening of *L* = 12.7 mm, Figure 3a shows isometric and plan views of pressure amplitude *p* in logarithmic scale on a plane of frequency *f* versus inflow velocity *U*. It is evident that sharply-defined peaks do not occur, which suggests the lack of generation of a flow tone. In both the isometric and plan views, however, the excitation of the acoustic modes is indeed evident. These modes are represented by crests on the isometric view and strips on the plan view respectively.

Although sharply-defined peaks are not evident at this small value of *L*, relatively broad, low-amplitude peaks are evident, and a linear fit through them is given by the thin white line as shown on the plan view of Figure 3a. At the location of each of these peaks, the corresponding hydrodynamic and acoustic modes are indicated. For example, *h1* represents the first hydrodynamic mode and *a1* represents the first acoustic mode. Evaluation indicates that the values of Q-factor of these peaks are very low, ranging from 40 to 130.

A further increase of length *L* of the cavity opening to *L* = 19.1 mm is represented by the plots of Figure 3b. In this figure it is evident that sharply defined peaks now occur, in contrast to the relatively broad peaks of the isometric views of Figure 3a. The plan view of Figure 3b shows the clearly-defined intersection of the hydrodynamic *h* and acoustic *a* modes, it is clear that the first two hydrodynamic modes (stages), i.e., *h1* and *h2* are clearly identifiable.

Correspondingly very large values of *Q* are attained, which occur for the first hydrodynamic mode *h1*, especially when these modes occur in conjunction with the third, fifth and seventh acoustic modes, i.e., *h1a3*, *h1a5* and *h1a7*. On the other hand, though the second hydrodynamic mode *h2* is detectable, its occurrence with the third, fifth and seventh modes yields only relatively low values of *Q* factor, the largest being *Q* = 140 at *h2a5*.

The maximum values of *Q* of the order of *Q* = 2,000 to 2,600 are, in fact, the largest values attainable, even for further increases in length *L* of the cavity opening. It therefore appears that this value of *L* = 19.1 mm represents the case of the strongest coupling

between the hydrodynamic instability of the shear layer associated with the acoustic *a* mode of the cavity resonator. A minimum value of *L* is required in order to allow the instability to adequately develop in the streamwise direction, and when this value of *L* is achieved, it is expected that optimal coupling will occur.

The next higher value of *L* of the cavity opening, *L* = 25.4 mm, is represented in Figure 3c. On the isometric view of Figure 3c, the peaks are sharply defined. On the plan view, the first and second hydrodynamic modes *h1* and *h2* are as indicated. It is evident that values of very high *Q*, which were evident for the previous case, *L* = 19.1 mm, persists. Again, values of *Q* of the order of 2,000 are attainable for the first hydrodynamic mode *h1*. Furthermore, the values of *Q* for the second hydrodynamic mode have become substantial. For example, for the intersection of the second hydrodynamic mode and the third acoustic mode *h2a3*, as well as with the fifth mode *h2a5*, values of *Q* = 620 and 980 are attained. Therefore, this longer value of cavity length has promoted much more sharply defined peaks of the second hydrodynamic mode.

A still larger value of length *L* of the cavity opening, *L* = 50.8 mm, is given in the plots of Figure 3d. As indicated in the plan view, it is now possible to define three hydrodynamic modes *h1* through *h3*. For the first hydrodynamic mode *h1* regions of relatively high pressure amplitude *p* extend over a significant range of inflow velocity *U*, at least at relatively large values of inflow velocity exceeding approximately 50 m/s. In contrast the second mode *h2* is excited over successively smaller ranges of *U*, with lower values of peak amplitude. Close inspection of the plan view of Figures 3d indicates that the third hydrodynamic mode *h3* is indeed detectable, and is therefore included in the present assessment.

Evaluation of *Q*-factor indicates that for the first hydrodynamic mode *h1*, the values of *Q* generally remain large, with the maximum value of *Q* of the order of *Q* = 1,800. But, on the average, these values are somewhat lower than for the previous (smaller) two values of *L*. On the other hand, for the second hydrodynamic mode *h2*, the values of *Q* have increased substantially to values of *Q* of the order of 1,000 to 1,300, which are significantly larger than the values of *Q* at the previous two smaller values of length *L*. Regarding the third hydrodynamic mode *h3*, values of *Q* generally remain small. We therefore witness the

increasing predominance of the second hydrodynamic mode as it couples with respective values of acoustic modes *a*, in particular, *h2a3* and *h2a5*.

The largest value of length L = 76.2 mm is indicated in Figure 3e. The basic form of the isometric plot of Figure 3e shows a fundamental change, relative to the form for smaller values of length L. A strong excitation occurs at a relatively low frequency of f = 168.0 Hz. Not only are the peak amplitudes large, but they extend over a substantial range of inflow velocity U and, in fact, are triggered at a relatively low value of U = 30 m/s.

The plan view of Figure 3e shows a series of four hydrodynamic modes. The classical three modes *h1*, *h2* and *h3* are designated. In addition, a special low frequency mode *h1**, which corresponds to the low frequency excitation at f = 168 Hz, and is also expected to occur at f = 495 Hz at higher values of velocity above current velocity range, is also designated.

The values of Q for the first hydrodynamic mode *h1* have degenerated to substantially lower values relative to those at smaller values of length L of the cavity opening. In the second hydrodynamic mode, *h2*, relatively high values of Q persist; that is, Q of the order of 1,000 is attainable. Important, however, is the fact that in the third hydrodynamic mode, *h3*, a relatively high value of Q = 760 is now attainable. This longer cavity length has apparently allowed nearly full evolution of the third hydrodynamic stage *h3*, and thereby a strongly coupled oscillation leading to a high value of Q.

Regarding the special low frequency mode, which is designated herein as *h1**, though it has a relatively large value of pressure amplitude p, its Q factor is not large, i.e., Q = 330.

An overview of the major pressure response peaks for the aforementioned values of length L of the cavity opening, as well as two additional values of L covered in the present investigation but not presented in the foregoing, is given in Figure 4. For a given value of streamwise length L, all pressure response peaks are superposed on the same coordinates p versus U. For example, compare the plot at the upper left of Figure 4 with the corresponding three-dimensional plots. Note, however, that pressure p in Figure 4 is presented on a linear scale, which differs from the logarithmic scale representation of p in those three-dimensional plots. It is evident by examination of the isometric representations

of Figure 3b that three well-defined (major) pressure response peaks can be identified. They all correspond to the first hydrodynamic mode *h1* and, furthermore, lie along the crests representing the third, fifth and seventh acoustic modes, i.e., *a3*, *a5* and *a7*. These three pressure response peaks are so designated in the upper left plot of Figure 4. The representations of the plot in the upper left of Figure 4 are based on curve fits through the data represented in Figure 3b. A similar type of representation holds for the remaining five plots given in Figure 4.

The advantage of this particular type of representation is that it allows a direct comparison of the peak amplitudes of the pressure response for increases in cavity length L. It also allows a direct comparison of the values of inflow velocity U at which each of the peaks occurs. For example, consider the top and middle plots as shown in the left column of Figure 4, which correspond to two different values of cavity length L. It is evident that the longer cavity length L = 25.4 mm allows much larger amplitude peaks, relative to the peak amplitudes at L = 19.1 mm. In addition, each of the mode combinations at L = 25.4 mm, i.e., *h1a3*, *h1a5* and *h1a7* require a higher value of inflow velocity U to generate the peak values. Furthermore, note that at successively larger values of L = 38.1 mm, 44.5 mm, 50.8 mm and 76.2 mm, the peak corresponding to the mode combination of *h1a3*, for example, occurs at successively larger values of inflow velocity U. It is interesting to observe, however, that the peak magnitude of this *h1a3* mode combination does not continue to increase with successively larger values of L and thereby larger values of U. Rather, it appears to saturate at about a level of p = 1,900 Pa at L = 50.8 mm and, in fact, experiences a substantial drop at L = 76.2 mm. This abrupt drop at L = 76.2 mm occurs in conjunction with the onset of the special mode combination $h1^{*}a1$, as well as increasingly larger contributions from the second hydrodynamic mode *h2*, principally in the form of *h2a5* and *h2a7*. Finally, it should be noted that the behavior of the pressure response of mode *h1a3* described in the foregoing is generally replicated by other mode combinations, such as *h1a1*, *h1a5*, and *h1a7*, especially the increase in value of U to excite them at increasing values of streamwise length L of the cavity. At the largest cavity length L = 76.2 mm, the peaks at *h1a1*, *h1a5*, *h1a7* are no longer detectable. Rather, the peak of this threshold mode

*h1*a1* dominates, along with the peaks at the second hydrodynamic mode, i.e., *h2a1*, *h2a5* and *h2a7*.

Table 1 gives an overview of the parameters corresponding to the peaks of Figure 4. For each combination of a hydrodynamic mode and an acoustic mode, such as the first hydrodynamic mode (stage) *h1* and the first acoustic mode *a1*, the following parameters are designated: inflow velocity *U*; frequency *f*; pressure amplitude *p*; dimensionless pressure amplitude normalized by the free stream dynamic head $p/0.5\rho U^2$; pressure amplitude $p/\rho Uc$ normalized by inflow velocity *U* and speed of sound *c*; strength of lock-on *SoL* (definition and detailed discussion are provided in Section 4); *Q* (quality)-factor; dimensionless frequency *fL/U* based on length *L* of cavity opening; and dimensionless frequency $f\theta/U$ based on momentum thickness θ of the inflow.

4. BACKGROUND LEVEL OF PRESSURE FLUCTUATION AND STRENGTH OF LOCK-ON

In Section 3, emphasis has been on the description of the organized peaks of pressure fluctuations that emerge above the background. These peaks, pronounced or not, are evident in the three-dimensional plots of the respective images of Figures 3a through 3e. An issue herein is how to measure the strength of flow tones represented by these peaks. Mendelson (2003) discusses in detail three methods. The first one is to subtract, on a decibel scale, the nonlinear modal response of the resonator to broadband flow noise from the resonant response during occurrence of a flow tone. The second method is to evaluate the quality factor *Q* of the pressure spectrum. The third is to define the strength in terms of the difference on a decibel scale between the peak of the pressure spectrum and the local broadband level of the spectrum.

Among these three methods, Mendelson (2003) states that the first one is the most tractable, as it is relatively easy to implement. The second method, while a valid measure, involves uncertainties due to finite resolution in the frequency domain; yet, it can be employed as an insightful approximation. Rockwell, Lin, Oshkai, Reiss and Pollack (2003) address this issue. The third method is difficult to apply, since the local broadband spectral response is largely governed by the location of the transducer.

In the following, efforts are dedicated to application of the first measure, which is designated as strength of lock-on *SoL*. In addition, a brief comparison between the first and the second measures is made at the end of this section.

4.1 EVALUATION OF BACKGROUND LEVEL

When a resonator is excited only by broadband fluid generated turbulence flow noise, it produces a response amplitude peak in the spectrum whose peak amplitude follows velocity U raised to a power n. Such broadband flow noise is known to act as a quadrapole (Lauchle, 1992). Experimentally it has been shown that the power n can be affected by many factors, including the geometric parameters of the resonator, resonant frequencies, as well as the properties of the fluid. In general, with all these conditions fixed, the response in decibels is governed by a linear relation

$$\text{Response (dB)} = \text{constant} + 20n\log U \ .$$

On a plot of response in decibels versus log of velocity, the above would appear as a straight line of slope $20n$. This straight line is referred to as background level, or broadband flow response.

During flow acoustic coupling, the nonlinear interaction between acoustic and hydrodynamic modes generates a modal response that emerges above the background level. In this case, a linear fit through those data points corresponding to decoupled response can be taken to represent this broadband flow response.

In order to systematically study the behavior of broadband flow response for turbulent shear flow past a deep cavity, plots of peak pressure amplitude p (in decibels) versus inflow velocity U on a logarithmic scale were considered. Each plot of this type corresponds to a selected acoustic mode of a specific deep cavity. All the responses of the deep cavities discussed in Section 3 were evaluated from this perspective. For each cavity configuration, only a limited number of acoustic modes were selected for process, without losing generality.

Figure 5 shows typical plots. The plots of the left column correspond to selected acoustic modes of cavity having length L = 25.4 mm and depth L_C = 482.6 mm, and the right column to modes of cavity having length L = 50.8 mm and depth L_C = 482.6 mm. In fact, each of these plots is related to a crest of the three-dimensional representation of

pressure amplitude in Figures 3c and 3d, which show pressure amplitude on a logarithmic scale as a function of frequency and velocity for a designated deep cavity. Each crest occurs for a given resonant acoustic mode along a narrow band of frequency; the central value of this band is regarded as the frequency of this resonant acoustic mode.

Based on such plots of p (in decibels) versus U on logarithmic scale, a linear fit can be made for each plot, using the approach discussed in the foregoing, to indicate the background level represented by each reference line. These fits are represented by the straight lines of Figure 5. It is evident that, for different acoustic modes of the same cavity, and for different cavities, the background level differs. A general form of the background level is given by

$$p_{BB} = p_{BB0} + 20n \log_{10} U ,$$

where p_{BB} denotes the pressure amplitude of the broadband flow response, p_{BB0} is the value of p_{BB} at $U = 1\,\text{m/s}$, and $20n$ is the slope of the linear fit, or, specifically, n denotes the exponent to U, keeping in mind that $U^n \propto p_{BB}$.

For all deep cavities and all selected acoustic modes, systematic evaluation of the amplitude p_{BB0} and exponent n has been conducted following the approach as indicated in Figure 5. Then in combination with curve fitting technique, a series of empirical formulas have been developed to estimate, or to predict, both p_{BB0} and n. Further study shows that these two parameters are a function of acoustic mode number n_a, cavity length L, and effective cavity depth L_{eff}. Detailed deduction and formularization have been provided by Yang (2005).

4.2 OVERVIEW OF FLOW TONES BASED ON STRENGTH OF LOCK-ON

Utilizing the empirical formulas discussed in the foregoing, estimation of the background level for a specified acoustic mode of a given cavity has now become quite simple and accurate. Strength of lock-on *SoL*, which is defined to subtract, on a decibel scale, the broadband flow response, i.e., the background level, from the nonlinear modal response of the resonator, is then systematically evaluated, for all the cavities discussed in Section 3 and for all the detectable peaks of each cavity.

To identify the occurrence of resonant flow tones, two criteria can be possibly applied. The first involves the quality Q factor of the predominant peak in the response spectrum of the pressure fluctuation, as discussed in Section 3; the other is strength of lock-on *SoL* criterion, which has so far been developed. For present investigation, the *SoL* criterion is employed. In essence, this *SoL* threshold is established as 40 dB. For purposes of comparison, based on a relatively large set of data acquired herein, *SoL* = 40 dB generally corresponds to a range of the quality factor of Q = 250 to 500 and to the range of raw pressure amplitude p = 50 to 200 Pa. Furthermore, it corresponds to the following ranges of dimensionless pressure amplitude response $0.04 \leq p/0.5\rho U^2 \leq 0.2$ and $0.004 \leq p/\rho Uc \leq 0.02$.

Upon attainment of the strength of lock-on *SoL* and establishment of resonance criterion, a three-dimensional bar graph has been created on the plane of cavity length L and ratio of acoustic mode number n_a to hydrodynamic mode number n_n, to show flow tone distribution of the entire cavity series, as presented in Figure 6.

In order to easily interpret the bar graph, or cone-like graph representation, given in Figures 6, it is helpful to clarify some key points related to their construction:

(i) The bar graph representation is for one series of cavities, and within the series, one particular cavity is represented by a shaded strip on the horizontal (bottom) plane.

(ii) On the horizontal (bottom) plane of each shaded strip, each intersection of two solid lines defines the intersection between the first hydrodynamic mode *h1* and a given acoustic mode. That is, all peaks related to the *h1* mode must be located at such intersections. Furthermore, these *h1* modes are further designated by the dark green cone. On the other hand, each intersection of two dashed lines defines the intersection between a second hydrodynamic mode *h2* and an acoustic mode, and all peaks related to the *h2* mode must be located at these intersections. Further, these *h2* modes are designated by the yellow cone. It should be noted that all possible peaks related to the third and higher hydrodynamic modes are not presented in this bar graph representation, since they were typically of much smaller amplitude.

(iii) Along the right edge of each plot, the ratio of the acoustic mode number to the hydrodynamic mode number is represented by n_a/n_h. These values are given as n_a/n_h =

1, 3, 5, …. Keeping in mind that the dark green cone corresponds to an *h1* mode with n_h = 1 and the yellow cone corresponds to the *h2* mode with n_h = 2, then the acoustic mode number n_a can be evaluated based on the indicated ratio n_a/n_h along the right edge of the plot.

(iv) For a given cavity, i.e., a given strip along the horizontal (bottom) plane, further study shows that the ratio of the acoustic mode number n_a to the hydrodynamic mode number n_h is proportional to the inflow velocity U. This means that for all of the cones of different colors located on the same shaded strip, the ratio n_a/n_h increases with an increase of U. Note, however, that the value of inflow velocity U to excite a mode at a given ratio n_a/n_h is different for each shaded strip on the horizontal (bottom) plane.

(v) Finally, amplitudes which exceed a threshold value of 40 dB are taken to represent a locked-on flow tone, i.e., a resonant peak. Such resonant peaks are presented by green or yellow cones with red tips, whereby the vertical extent of the red region represents the excess of the strength of lock-on *SoL* relative to the threshold of 40 dB.

As shown in Figure 6, it is evident that with an increase of the length L of the cavity opening, the strongest attainable strength of lock-on SoL reaches a maximum, then starts to decrease. More specifically, for the peaks related to the first hydrodynamic mode *h1*, there is no locked-on flow tone generated for $L \le 15.9\,\text{mm}$; for $L \ge 19.1\,\text{mm}$, locked-on flow tones start to occur and the most pronounced one is observed at $L = 25.4\,\text{mm}$. In contrast, for those peaks related to the second hydrodynamic mode *h2*, locked-on flow tones first occur at $L = 25.4\,\text{mm}$ and show the peak at $L = 50.8\,\text{mm}$.

The physics behind the foregoing patterns of peaks for both hydrodynamic modes is as follows. During the interaction, or coupling, of an acoustic mode with a hydrodynamic mode, the fluctuating shear layer needs a sufficient streamwise length to adequately develop. For small values of L, the fluctuation of the shear layer is suppressed, and the response is weak. As L increases, the fluctuation becomes more amplified, yielding larger amplitude response, represented by higher values of SoL. This trend continues until the value of SoL reaches the maximum. The value of L corresponding to this maximum is herein referred to as the optimal length of the cavity opening for generation of flow tones. After that, a further increase of L does not cause a remarkable change of the peak pressure

amplitude *p*, but the intersection of the same acoustic mode with the same hydrodynamic mode will occur at a higher inflow velocity *U*, which provides a higher background level, and consequently yield a lower value of SoL. Furthermore, for the *h2* mode, the optimal length *L* of the cavity opening is twice as large as for the *h1* mode, since it is expected that two wavelengths of the fluctuating shear layer fit in the streamwise length of the cavity opening for the *h2* mode instead of one wavelength for the *h1* mode.

Comparison of the SoL for different hydrodynamic modes shows that, for a given deep cavity, the *h1* mode is always predominant over other hydrodynamic modes. On each shaded strip, peaks in dark green are generally much higher than peaks in yellow, no matter whether they are resonant or not. Yet, an exception is observed. For the deep cavity of depth $L_C = 482.6\,\text{mm}$ and length $L = 76.2\,\text{mm}$, an *h1* mode *h1a1* should be preferentially excited, but is missing, as marked by a dark blue ellipse in the bar graph. Although another *h1* mode *h1a3* is detected, the value of the SoL is much lower than the *h2* modes. The reason behind this irregular behavior is that a special hydrodynamic mode, even lower than the *h1* mode, occurs. This extra low hydrodynamic mode is designated as the *h1** mode, and has been discussed in the foregoing Section 3.

The top plot of Figure 7 shows the strength of lock-on SoL_{max}, which represents the strongest flow tone for a designated hydrodynamic mode *h* of a given cavity, as a function of dimensionless streamwise length L/θ of the cavity, in which θ is the momentum thickness of the inflow boundary layer. Three different curves are shown, each for a given hydrodynamic mode *h1*, *h2* and *h3*. For each view of *h*, when L/θ becomes sufficiently small, the magnitude of SoL_{max} becomes very small. For the lowest two hydrodynamic modes, *h1* and *h2*, rapid increases of SoL_{max} occur in the range of L/θ from approximately 30 to 45. More specifically, the values of SoL_{max} exceed the threshold 40 dB in the range of L/θ from 32 to 42, then appear to plateau. In contrast, corresponding variation for the third hydrodynamic mode *h3* presents a much milder variation with L/θ and, furthermore, this mode *h3* is apparent only at a sufficiently large value of L/θ, for which approximately three wavelengths of the instability along the cavity length *L* can occur.

The lower plot of Figure 7 shows the corresponding dimensionless frequency $f\theta/U$ as a function of L/θ. These variations are shown for the three hydrodynamic modes *h1*, *h2* and *h3*. At the right of this plot, the dimensionless amplification factor $-\alpha_i\theta$ versus $f\theta/U$, taken from Michalke (1965), is plotted in such a fashion that one can compare directly with the experimentally observed values of $f\theta/U$, i.e., with the filled circle, diamond and triangular symbols. It is interesting to compare the values of L/θ at which a threshold value of SoL_{max} is attained in the top plot of Figure 7. These values are designated by the dashed circles surrounding the indicated data points, all of which occur in the vicinity of the aforementioned cut-off criterion $SoL_{max} \geq 40$ dB. If these encircled data points are compared with the corresponding encircled points in the bottom plot of $f\theta/U$, it is evident that all three of these dimensionless frequencies fall in a range that corresponds to a relatively large set of values of $-\alpha_i\theta$. A relatively high $-\alpha_i\theta$ predicted from a linear stability theory indicates that the preferred frequency of the shear layer oscillation, which also yields the highest amplitude SoL_{max} of the oscillation, occurs at relatively high values of $-\alpha_i\theta$ of the inherent hydrodynamic instability of the shear flow past the cavity.

4.3 COMPARISON OF MEASURES OF STRENGTH OF FLOW TONES

For the plots of pressure amplitude p in dB versus inflow velocity U on a logarithmic scale, as shown in Figure 5, subtraction of the background level p_{BB} (in dB) from p (in dB) yields another family of plots: strength of lock-on SoL versus inflow velocity U. Unlike previous descriptions, which focus only on local peaks, the new plots show more details of low level response, as well as the development of peaks. As an effective measure of the strength of flow tones, a typical representation of variation of SoL as a function of U for the first through the seventh acoustic modes *a1* through *a7* is provided in Figure 8, which is related to the deep cavity of length L = 25.4 mm and depth L_C = 482.6 mm. As an alternative measure, the variation of corresponding values of quality factor Q as a function of U is also provided in this figure.

Comparison of the profile of SoL with the profile of Q shows that they generally agree well, especially in describing the development of the local peaks. These peaks are

marked by the dashed lines on each plot. Each peak represents an intersection between a designated acoustic mode, e.g., *a1*, and the first *h1* or the second *h2* hydrodynamic mode. The *h1* mode peaks occur at relatively high velocities, and the *h2* mode peaks occur at lower velocities, if they are detectable.

Instead of the foregoing comparison between the two measures, a quantitative comparison can also be made by computing the *Q* factor in decibels relative to a reference level. Mendelson (2003) suggests that in order to obtain agreement on both measures, it is necessary to choose an appropriate reference for the *Q* factor. This reference *Q* factor should be derived from a case without flow-acoustic coupling. However, preliminary experiments, which were conducted by means of white noise excitation and spoiled shear flow past the deep cavity, showed that values of such *Q* factor varied significantly. Therefore it is difficult to establish a criterion to choose such a reference level.

Taken together, the similar trends of the parameters SoL and *Q* verifies that both measures are equivalent; the difficulty of evaluating the *Q* factor in dB relative to a reference level makes the SoL measure a better choice.

5. CONCLUSIONS

Self-excited instabilities arising from flow past a deep cavity have been investigated for the case where the cavity functions as an isolated element, i.e., the possibility of coupling with an inflow or outflow duct is precluded.

When coupling occurs between an unstable hydrodynamic mode (stage) *h* of the unstable shear layer along the cavity and an acoustic mode *a* of the deep cavity, the potential exists for a strongly coupled oscillation in the form of a pronounced flow tone. The pressure amplitude response of the resonant cavity, in relation to the initial onset, development, and attainment of the coupled flow tone, via variations of the inflow velocity, has been pursued for a range of streamwise length L of the cavity opening at a constant depth L_C of the cavity. Detailed three-dimensional plots showing the pressure response characteristics have been acquired for this cavity series. This approach allows classification of the response in terms of the large array of possible intersections of hydrodynamic modes

h and acoustic modes *a*. Furthermore, features of the turbulent (random) background level, away from the conditions corresponding to the onset of a flow tone, have been determined in relation to the streamwise length L of the cavity and the cavity depth L_C. With this background level as a reference, the strength of lock-on *SoL* can be quantified. In the following, brief summaries of these aspects are given.

5.1 CRITERION FOR LOCKED-ON FLOW TONES

Two appropriate criteria for characterization of a locked-on flow tone have been examined in detail. The first criterion is the quality factor Q of the spectral peak of the pressure response, defined as $Q = f_0/(f_2 - f_1)$, in which f_0 is the frequency of the tone, and f_1 and f_2 are the frequencies at the half-power points of the spectral peak. The value of Q can be rapidly estimated, subject to uncertainties associated with finite resolution in the frequency domain. The second criterion is strength of lock-on *SoL*, which represents the excess amplitude of the spectral peak with respect to the background noise level. This approach requires evaluation of the background level over a substantial range of inflow velocity, and therefore is time consuming to evaluate, but somewhat more accurate than the Q factor criterion. Based on the wide range of pressure response characteristics considered herein, a value of *SoL* = 40 dB was selected to represent the threshold value for a locked-on flow tone. This value of *SoL* corresponds to values of quality factor in the range $250 \leq Q \leq 500$. Furthermore, it corresponds to the following ranges of dimensionless pressure amplitude response $0.04 \leq p/0.5\rho U^2 \leq 0.2$ and $0.004 \leq p/\rho Uc \leq 0.02$.

5.2 PRESSURE RESPONSE CHARACTERISTICS DUE TO VARIATIONS OF CAVITY LENGTH AT CONSTANT CAVITY DEPTH

Variation of the streamwise length L of the cavity yields the following regimes of response.

(i) Below a given value of L, no flow tones are attainable. This value of L is defined as L_{min}, normalized by the momentum thickness θ, which is evaluated at the velocity U of interest. These values of minimum dimensionless length lie in the range of $32 \leq L_{min}/\theta \leq 42$; the particular value depends upon the hydrodynamic mode (stage) of the oscillation.

(ii) When the cavity length initially exceeds the value of L_{min}/θ, the first hydrodynamic mode (stage) *h1* is dominant; it couples with the acoustic modes *a3, a5* and *a7*. Flow tones are not generated in the second hydrodynamic mode (stage) *h2*, but these peaks are well defined at the intersections with acoustic modes *a3, a5,* and *a7*.

(iii) When L/θ becomes sufficiently large, L/θ = 36, flow tones occur at the intersections of the first hydrodynamic mode (stage) *h1* with the *a1* through *a7* modes; the second hydrodynamic mode (stage) *h2* occurs in conjunction with selected acoustic modes over this range.

(iv) At still larger values of L/θ = 58, the first and second hydrodynamic modes (stages) *h1* and *h2* selectively show locked-on flow tones at certain values of acoustic modes in the range *a1* through *a7*. The third hydrodynamic mode (stage) *h3* is detectable, and can attain large values of strength of lock-on *SoL*, but does not attain the level defined as a flow tone.

(v) At L/θ = 110, a special, sub-first hydrodynamic mode (stage) $h1^*$ generates a flow tone in conjunction with the first acoustic mode *a1*. This $h1^*$ mode has a dimensionless frequency nearly two-thirds that of the classical *h1* mode. Furthermore, at this value of L/θ, the second hydrodynamic mode *h2* can generate a flow tone, whereas modes *h1* and *h3*, though attaining reasonably high values of *SoL*, do not generate tones.

5.3 MINIMUM CAVITY LENGTH FOR ONSET OF OSCILLATION: CONCEPTUAL MODEL

As indicated in the foregoing, there exists a minimum cavity length L_{min}/θ, for which onset of a flow tone can occur; that is, in order for the amplitude of the pressure response peak to exceed the threshold value of strength of lock-on *SoL*, it is necessary for the value of L/θ to be sufficiently large. By considering the variations of *SoL* versus the streamwise length L/θ of the cavity for each of the hydrodynamic modes *h1, h2* and *h3*, and also considering the values of dimensionless frequency in the form $f\theta/U$ versus L/θ for each of the hydrodynamic modes *h1, h2* and h3, then cross-comparing with the variation of amplification factor $-\alpha_i\theta$ versus $f\theta/U$ based on the linear stability theory, it is possible to demonstrate that the strength of lock-on *SoL* for onset of a flow tone, corresponding to

attainment of a sufficiently large L/θ, is in accord with the band of most amplified disturbances in the developing shear layer, i.e., the largest values of $-\alpha_i\theta$.

ACKNOWLEDGEMENTS

The authors gratefully acknowledge the advice of Professor Peter Oshkai, presently at the University of Victoria, while holding a post-doctoral position at Lehigh University.

REFERENCES

Blake, W. K. 1986 Mechanics of Flow-Induced Sound and Vibration, Vols. 1 and 2. Academic Press, Inc., NY.

Bruggeman, J. C. 1987 “Flow-Induced Pulsations in Pipe Systems”, Doctoral Dissertation, Technical University of Eindhoven.

Bruggeman, J. C., Hirschberg, A., van Dongen, M. E. H., Wijnands, A. P. J. & Gorter, J. 1989 “Flow Induced Pulsations in Gas Transport Systems: Analysis of the Influence of Closed Side Branches”. *Journal of Fluids Engineering*, **111**, 484-491.

Bruggeman, J. C., Hirschberg, A., van Dongen, M. E. H., Wijnands, A. P. J. & Gorter, J. 1991 “Self-Sustained Aero-Acoustic Pulsations in Gas Transport Systems: Experimental Study of the Influence of Closed Side Branches”. *Journal of Sound and Vibration*, **150**, 371-393.

Cremer, L. & Ising, H. 1967 “Die Selbsterregten Schwingungen Von Orgelpfeifen.” *Acustica*, **19**, 143-153.

Cumpsty, N. S. & Whitehead, D. S. 1971 "The Excitation of Acoustic Resonances by Vortex Shedding", *Journal of Sound and Vibration*, **18**(3), 353-369.

Davies, P. O. A. L. 1981 "Flow-Acoustic Coupling in Ducts", *Journal of Sound and Vibration*, **77**(2), 191-209.

Davies, P. O. A. L. 1996a "Piston Engine Intake and Exhaust System Design", *Journal of Sound & Vibration*, **190**, 677-712.

Davies, P. O. A. L. 1996b "Aeroacoustics and Time Varying Systems", *Journal of Sound and Vibration*, **190**, 345-362.

DeMetz, F. C. & Farabee, T. M. 1977 “Laminar and Turbulent Shear Flow-Induced Resonances”, AIAA Paper 77-1293.

Dequand, S. 2001 “Duct Aeroacoustics: From Topological Applications to the Flute”, Doctoral Dissertation, Technical University of Eindhoven.

Elder, S. A. 1978 “Self-Excited Depth-Mode Resonance for a Wall-Mounted Cavity in Turbulent Flow”, *Journal of Acoustical Society of America*, **64**, 877-890.

Flatau, A. & Van Moorhem, W. K. 1990 "Prediction of Vortex Shedding Responses in Segmented Solid Rocket Motors", AIAA Paper 90-2073.

Fletcher, N. H. 1974 "Nonlinear Interactions in Organ Flue Pipes", *Journal of the Acoustical Society of America*, **56**(2), 645-652.

Fletcher, N. H. 1976 "Sound Production by Organ Flue Pipes", *Journal of the Acoustical Society of America*, **60**(4), 926-936.

Fletcher, N. H. 1979 "Air Flow and Sound Generation in Musical Wind Instruments", *Annual Review of Fluid Mechanics*, **11**, 123-146.

Geveci, M., Oshkai, P., Rockwell, D., Lin, J.-C. & Pollack, M. 2003 "Imaging of the Self-Excited Oscillation of Flow Past a Cavity during Generation of a Flow Tone", *Journal of Fluid and Structures*, **18**(6), 665-694.

Hofmans, G. C. J. 1998 "Vortex Sound in Confined Flows", Doctoral Dissertation, Technical University of Eindhoven.

Hourigan, K., Welsh, M. C., Thompson, M. C. & Stokes, A. N. 1990 "Aerodynamic Sources of Acoustic Resonance in a Duct with Baffles". *Journal of Fluids and Structures*, **4**, 345-370.

Howe, M. S. 1975 "Contributions to the Theory of Aerodynamic Sound, with Application to Excess Jet Noise and Theory of the Flute", *Journal of Fluid Mechanics*, **71**, 625-673.

Howe, M. S. 1980 "The Dissipation of Sound at an Edge", *Journal of Sound and Vibration*, **70**, 407-411.

Ingard, U. & Singhal, V. K. 1976 "Flow Excitation and Coupling of Acoustic Modes of a Side-Branch Cavity in a Duct", *Journal of the Acoustical Society of America*, **60**, 1213-1215.

Jungowski, W.M., Botros, K.K., and Studzinski, W. 1989 "Cylindrical Side-Branch as Tone Generator", *Journal of Sound and Vibration*, **131**, 265-285.

Kriesels, P. C., Peters, M. C. A. M., Hirschberg, A., Wijnands, A. P. J., Iafrati, A., Riccaradi, G., Piva, R. & Bruggeman, J. C. 1995 "High Amplitude Vortex-Induced Pulsations in a Gas Transport System", *Journal of Sound and Vibration*, **184**, 343-368.

Lauchle, G. C. 1992 Modern Methods in Analytic Acoustics: Lecture Notes. Springer-Verlag.

Mendelson, R. S. 2003 "Methods of Measuring Lock-in Strength and Their Application to the Case of Flow over a Cavity Locking into a Single Side Branch", AIAA Paper 2003-3106.

Michalke, A. 1965 “On Spatially Growing Disturbances in an Inviscid Shear Layer”, *Journal of Fluid Mechanics*, **23**, 521-544.

Nelson, P. A., Halliwell, N. A. & Doak, P. E. 1981 “Fluid Dynamics of a Flow Excited Resonance. Part I: Experiment”, *Journal of Sound and Vibration*, **78**, 15-38.

Nelson, P. A., Halliwell, N. & Doak, P. E. 1983 “Fluid Dynamics of a Flow Excited Resonance, Part II: Flow Acoustic Interaction”, *Journal of Sound and Vibration*, **91**, 375-402.

Oshkai, P., Geveci, M., Rockwell, D. & Pollack, M. 2004 “Imaging of Acoustically Coupled Oscillations Due to Flow Past a Shallow Cavity: Effect of Cavity Length Scale”, *Journal of Fluids and Structures*, in press.

Parker, R. 1966 "Resonance Effects in Wake Shedding from Parallel Plates: Some Experimental Observations", *Journal of Sound and Vibration*, **4**, 62-72.

Pfizenmaier, E. 1973 "On the Instability of a Sound Influenced Free Jet", *E.S.R.O. Technical Transl*, No. 122 (Transl. of *DFVLR Berlin Rep*. DLR-FB 73-69*).*

Rockwell, D. & Naudascher, E. 1978 "Review - Self-Sustaining Oscillations of Flow Past Cavities", Transactions of the ASME, *Journal of Fluids Engineering*, **100**, 152-165.

Rockwell, D. & Naudascher, E. 1979 "Self-Sustained Oscillations of Impinging Free-Shear Layers", *Annual Review of Fluid Mechanics*, **11**, 67-94.

Rockwell, D. & Schachenmann, A. 1982a “Self-Generation of Organized Waves in an Impinging Turbulent Jet at Low Mach Number”, *Journal of Fluid Mechanics*, **117**, 425-441.

Rockwell, D. & Schachenmann, A. 1982b “The Organized Shear Layer Due to Oscillations of a Turbulent Jet through an Axisymmetric Cavity”, *Journal of Sound and Vibration*, **85**, 371-382.

Rockwell, D. & Karadogan, H. 1982 H. "Oscillations of an Impinging Turbulent Jet: Coherence Characterization via Conditional Sampling", *Journal of Sound and Vibration*, **83**(1), 111-124.

Rockwell, D. & Karadogan, H. 1983 "Toward Attenuation of Self-Sustained Oscillations of a Turbulent Jet through a Cavity", ASME *Journal of Fluids Engineering*, **105**(3), 335-340.

Rockwell, D. 1983 “Oscillations of Impinging Shear Layers”. Invited Lecture, 20th Aerospace Sciences Meeting of AIAA, January, 1981, Orlando, FL; AIAA Paper 81-0047; also see *AIAA Journal*, **21**, 645-664.

Rockwell, D. 1998 “Vortex-Body Interactions”, *Annual Review of Fluid Mechanics*, **30**, 199-229.

Rockwell, D., Lin, J.-C., Oshkai, P., Reiss, M. & Pollack, M. 2003 “Shallow Cavity Flow Tone Experiments: Onset of Locked-on States”, *Journal of Fluids and Structures*, **17**, 381-414.

Schachenmann, A. & Rockwell, D. 1980 “A Quasi-standing-wave Phenomenon Due to Oscillating Internal Flow”, *Journal of Fluids Engineering*, **102**, 70-77.

Stoneman, S. A. T., Hourigan, K., Stokes, A. N. & Welsh, M. E. 1988 "Resonant Sound Caused by Flow Past Two Plates in Tandem in a Duct", *Journal of Fluid Mechanics*, **192**, 455-484.

Yang, Y. 2005 "Generation of Tones Due to Grazing Shear Flow Past a Deep Cavity” Doctoral Dissertation, Lehigh University.

Ziada, S. & Bühlmann, E. T. 1992 “Self-Excited Resonances of Two-Side-Branches in Close Proximity”, *Journal of Fluids and Structures*, **6**, 583-601.

LIST OF FIGURES

Symbols *h1* and *h2* correspond to the first and the second hydrodynamic modes (stages), with n_h = 1 and 2 respectively. Cavity depth corresponds to L_C = 482.6 mm.

Figure 7: Variation of strength of lock-on SoL_{max} at the maximum deviation of pressure amplitude from the reference line as a function of streamwise length L of the cavity opening normalized by the momentum thickness θ of the inflow boundary layer (top plot), and variation of dimensionless frequency $f\theta/U$ as a function of L/θ (bottom plot) in comparison with theoretically determined value of normalized amplification factor $-\alpha_i\theta$ versus $f\theta/U$ (from Michalke, 1965). The cavity depth is of a fixed value L_C = 482.6 mm.

Figure 8: Strength of lock-on *SoL* as a function of inflow velocity U in comparison with corresponding values of quality factor Q as a function of inflow velocity U for the first through the seventh acoustic modes *a1* through *a7*. Streamwise cavity length L = 25.4 mm, cavity depth L_C = 482.6 mm.

LIST OF TABLES

Table 1: Modes and parameters corresponding to the plots of Figure 4. Mode *h1a1* represents the coincidence of the first hydrodynamic mode (first stage) *h1* of oscillation of the shear layer and the first acoustic mode *a1* of the deep cavity. A similar designation holds for other hydrodynamic and acoustic modes. For each of these combinations, raw and dimensionless values of frequency f and amplitude p of each respective spectral peak are tabulated. In addition, the strength of lock-on *SoL* is given.

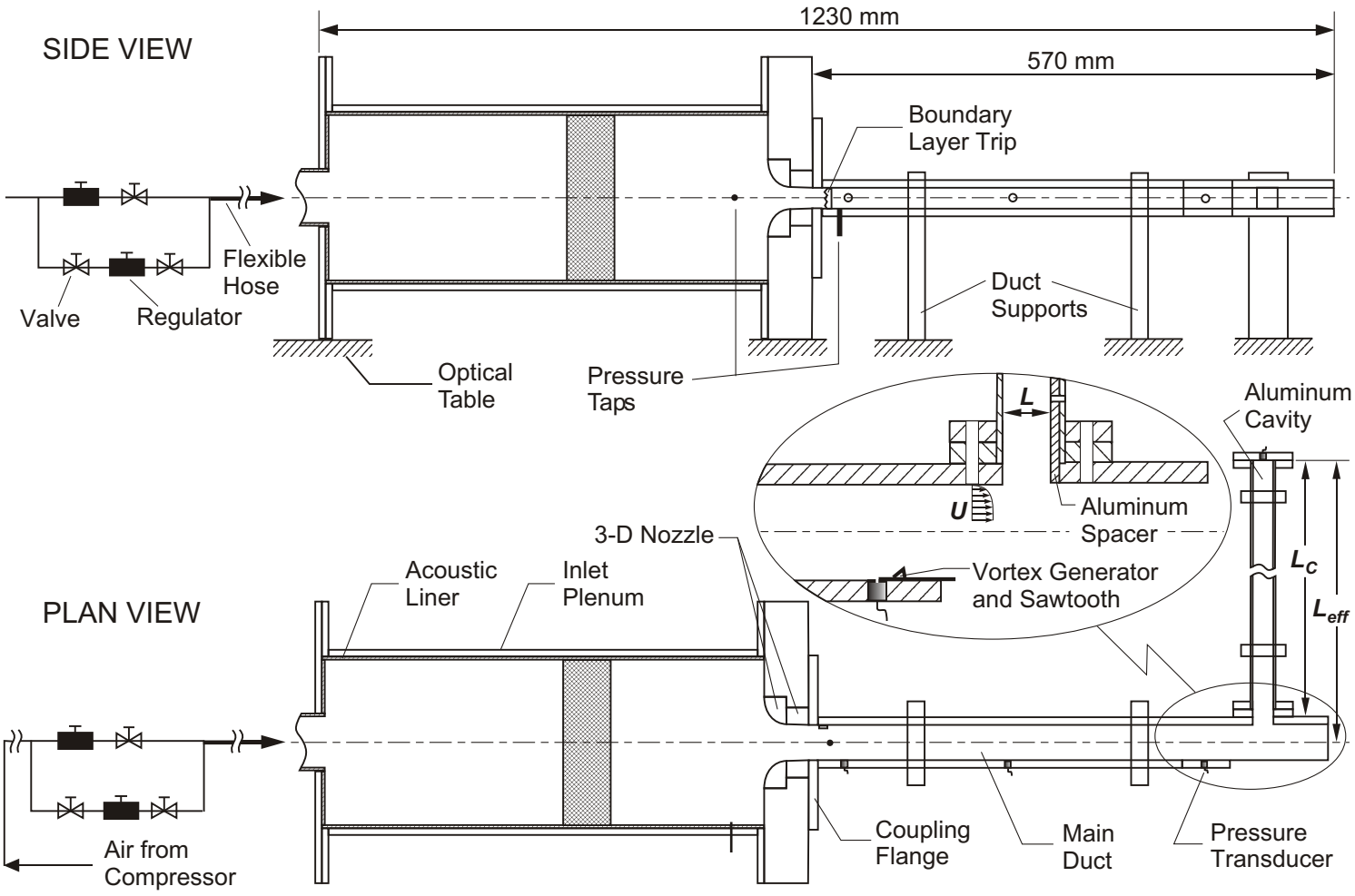

Figure 1: Overview of deep cavity facility.

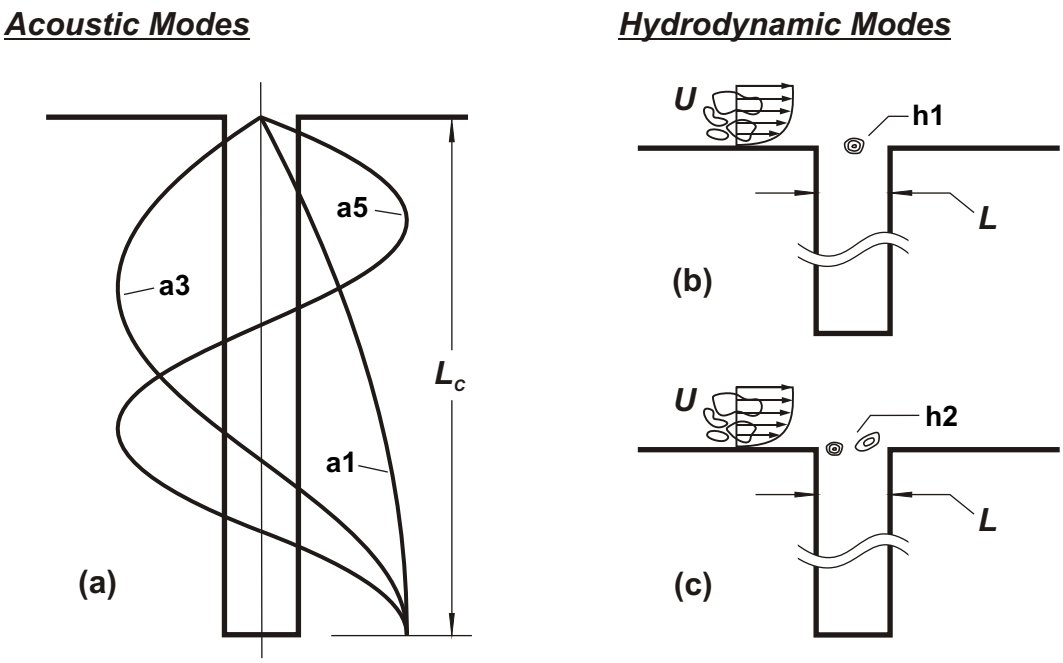

Figure 2: Schematics demonstrating acoustic modes (left) and hydrodynamic modes (right).

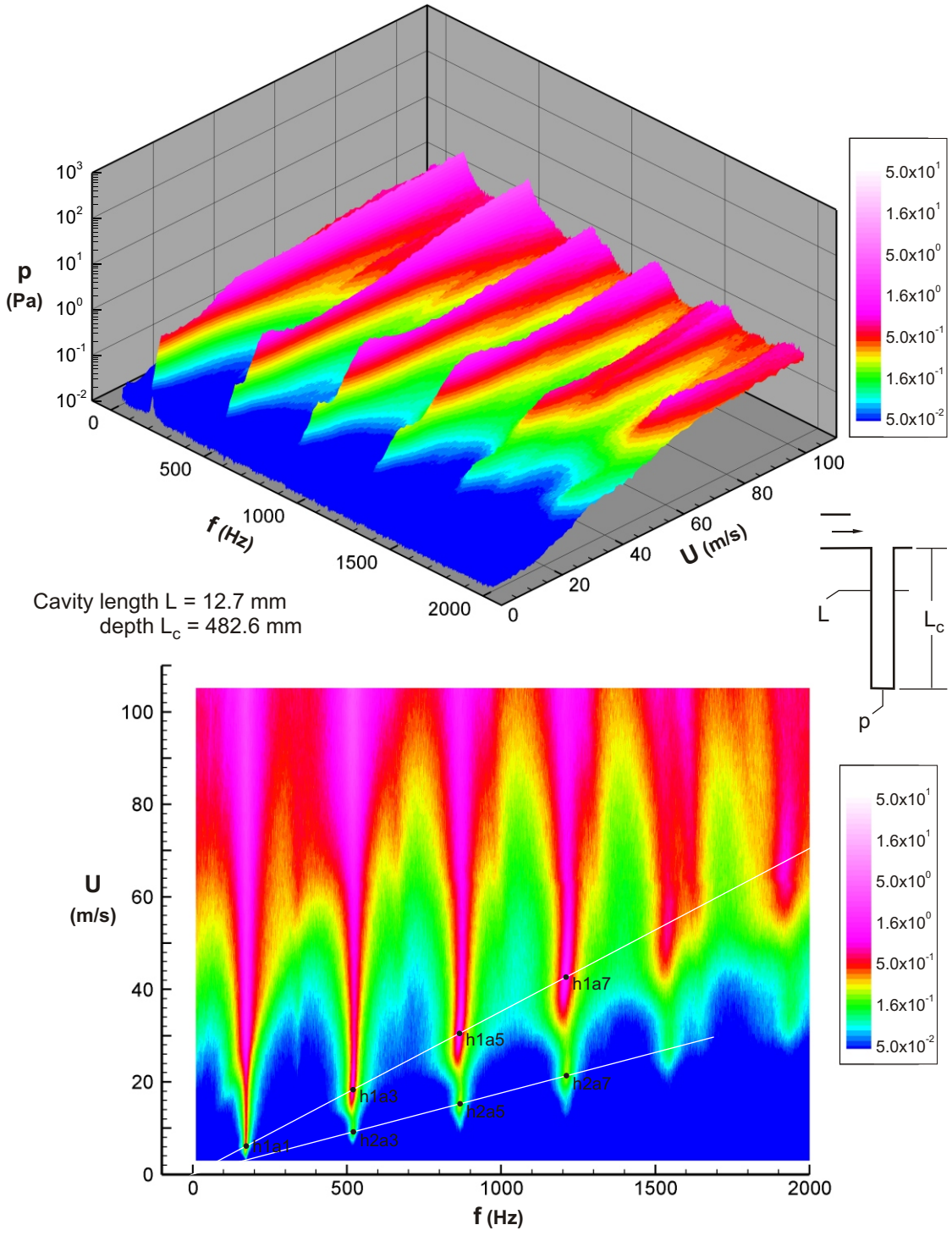

Figure 3a: Three-dimensional (top) and plan (bottom) views of pressure amplitude on a logarithmic scale as a function of frequency and velocity. Inflow velocity is varied while cavity geometry remains fixed. The plots were constructed from individual spectra of the pressure fluctuation at discrete values of velocity. Cavity length L and depth L_c are $L = 12.7$ mm and $L_c = 482.6$ mm.

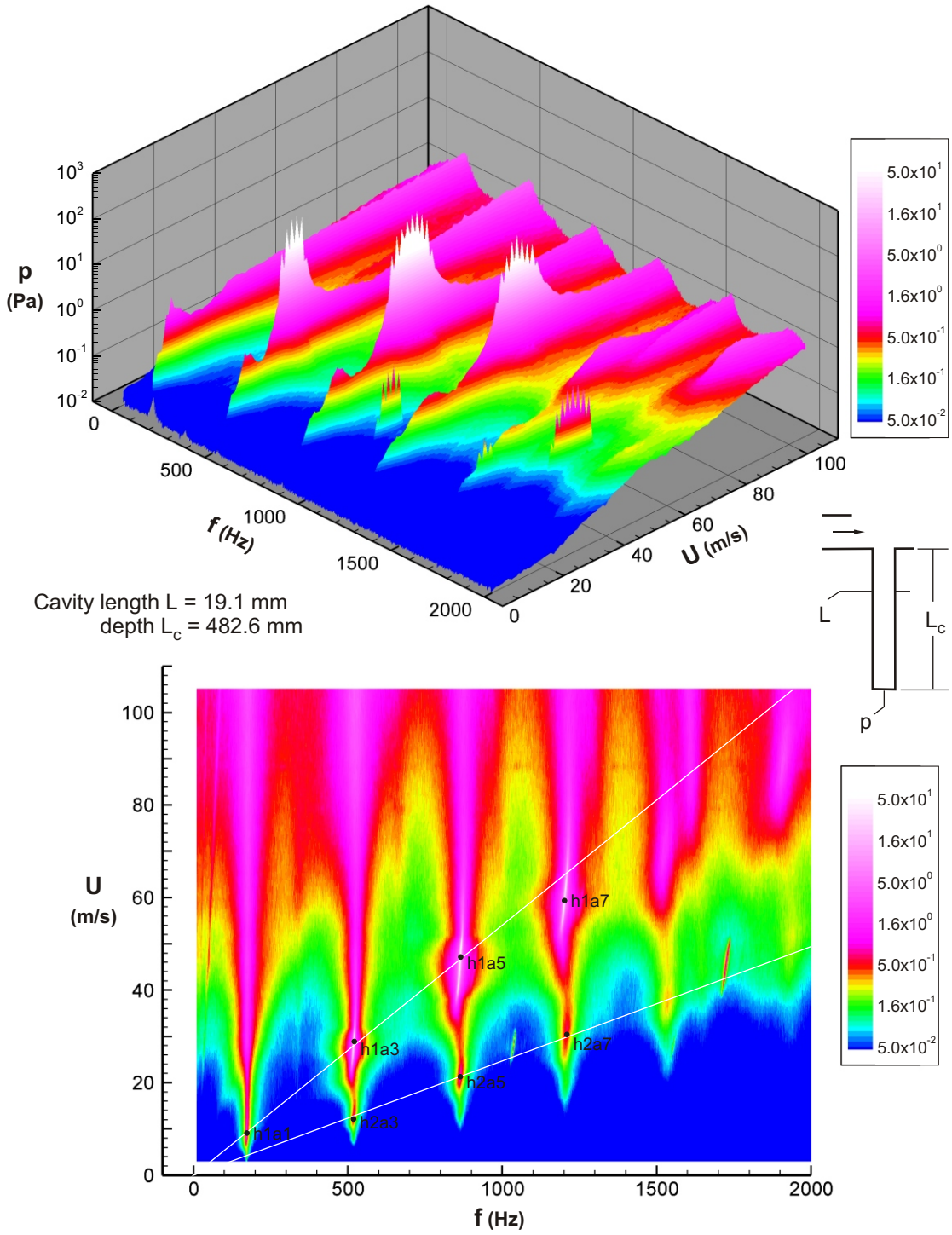

Figure 3b: Three-dimensional (top) and plan (bottom) views of pressure amplitude on a logarithmic scale as a function of frequency and velocity. Inflow velocity is varied while cavity geometry remains fixed. Cavity length L and depth L_c are $L = 19.1$ mm and $L_c = 482.6$ mm.

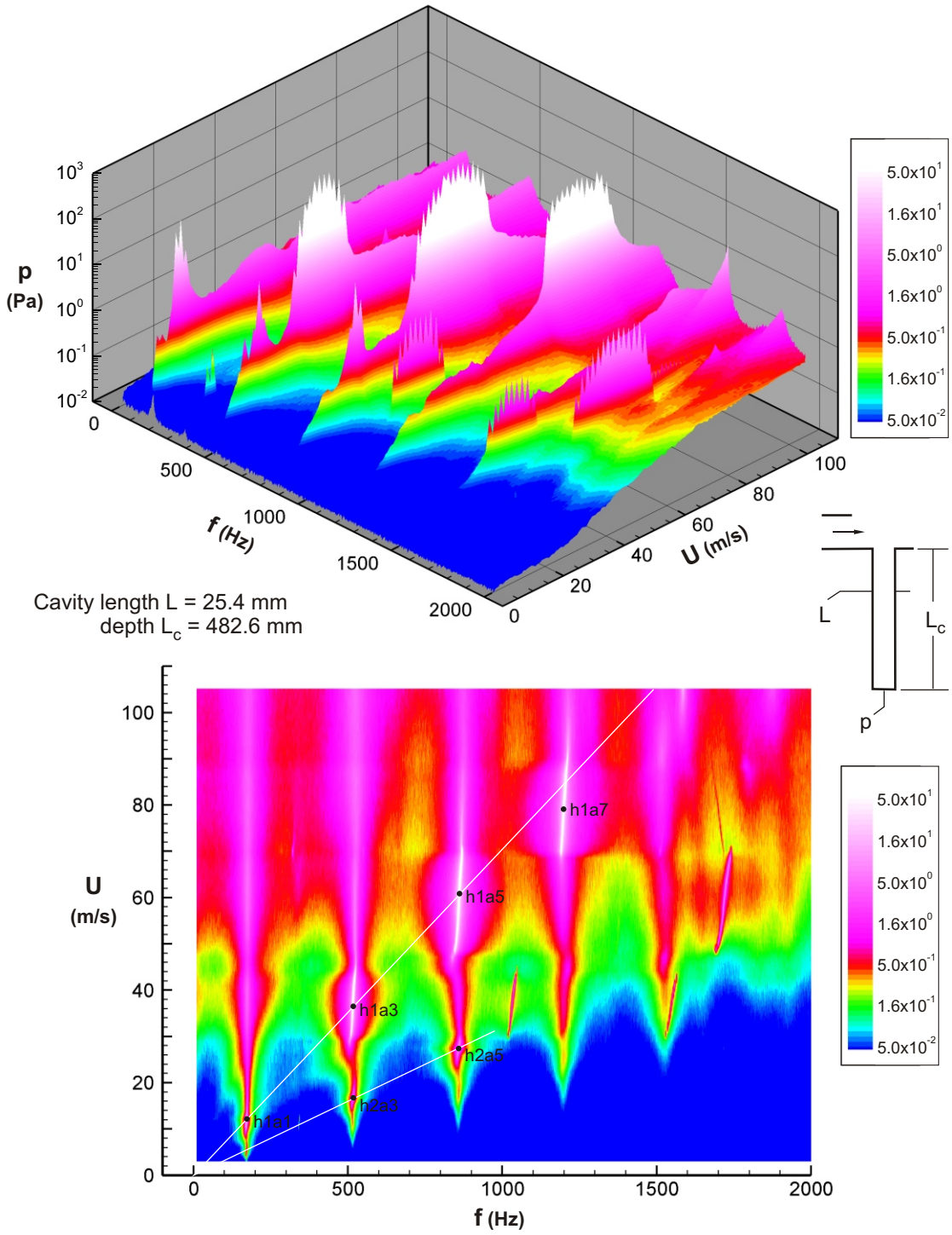

Figure 3c: Three-dimensional (top) and plan (bottom) views of pressure amplitude on a logarithmic scale as a function of frequency and velocity. Inflow velocity is varied while cavity geometry remains fixed. Cavity length L and depth L_c are $L = 25.4$ mm and $L_c = 482.6$ mm.

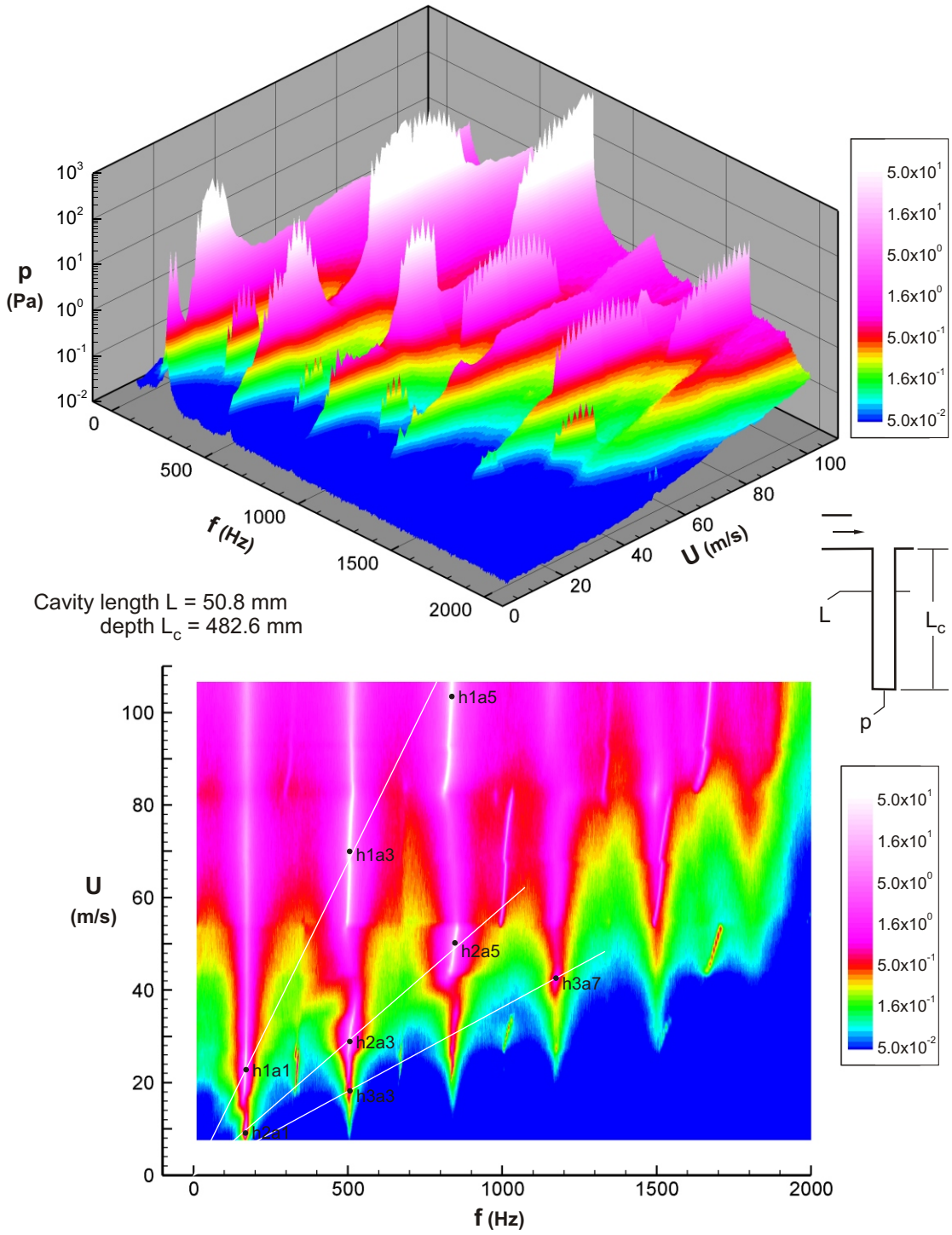

Figure 3d: Three-dimensional (top) and plan (bottom) views of pressure amplitude on a logarithmic scale as a function of frequency and velocity. Inflow velocity is varied while cavity geometry remains fixed. Cavity length L and depth L_c are $L = 50.8$ mm and $L_c = 482.6$ mm.

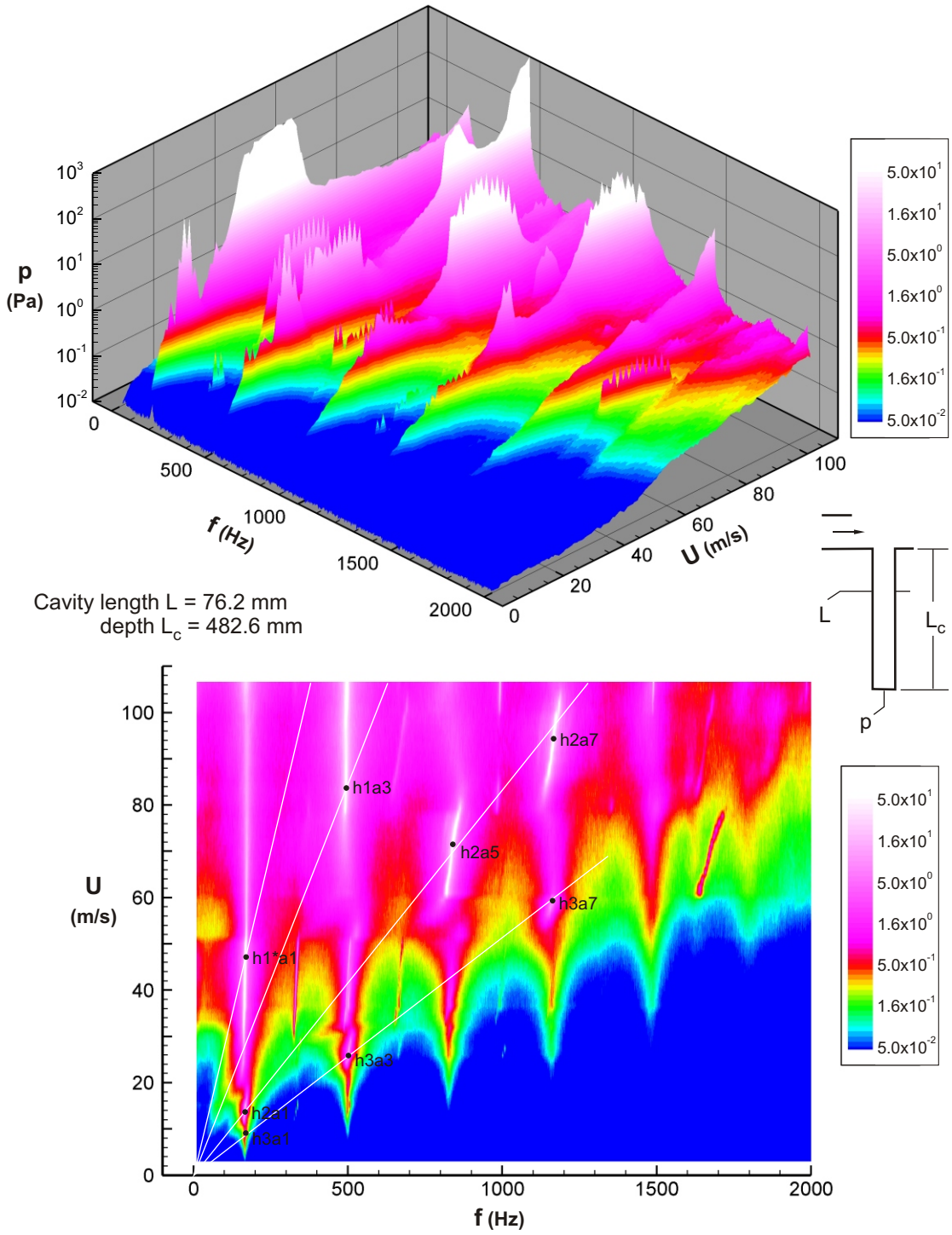

Figure 3e: Three-dimensional (top) and plan (bottom) views of pressure amplitude on a logarithmic scale as a function of frequency and velocity. Inflow velocity is varied while cavity geometry remains fixed. Cavity length L and depth L_c are $L = 76.2$ mm and $L_c = 482.6$ mm.

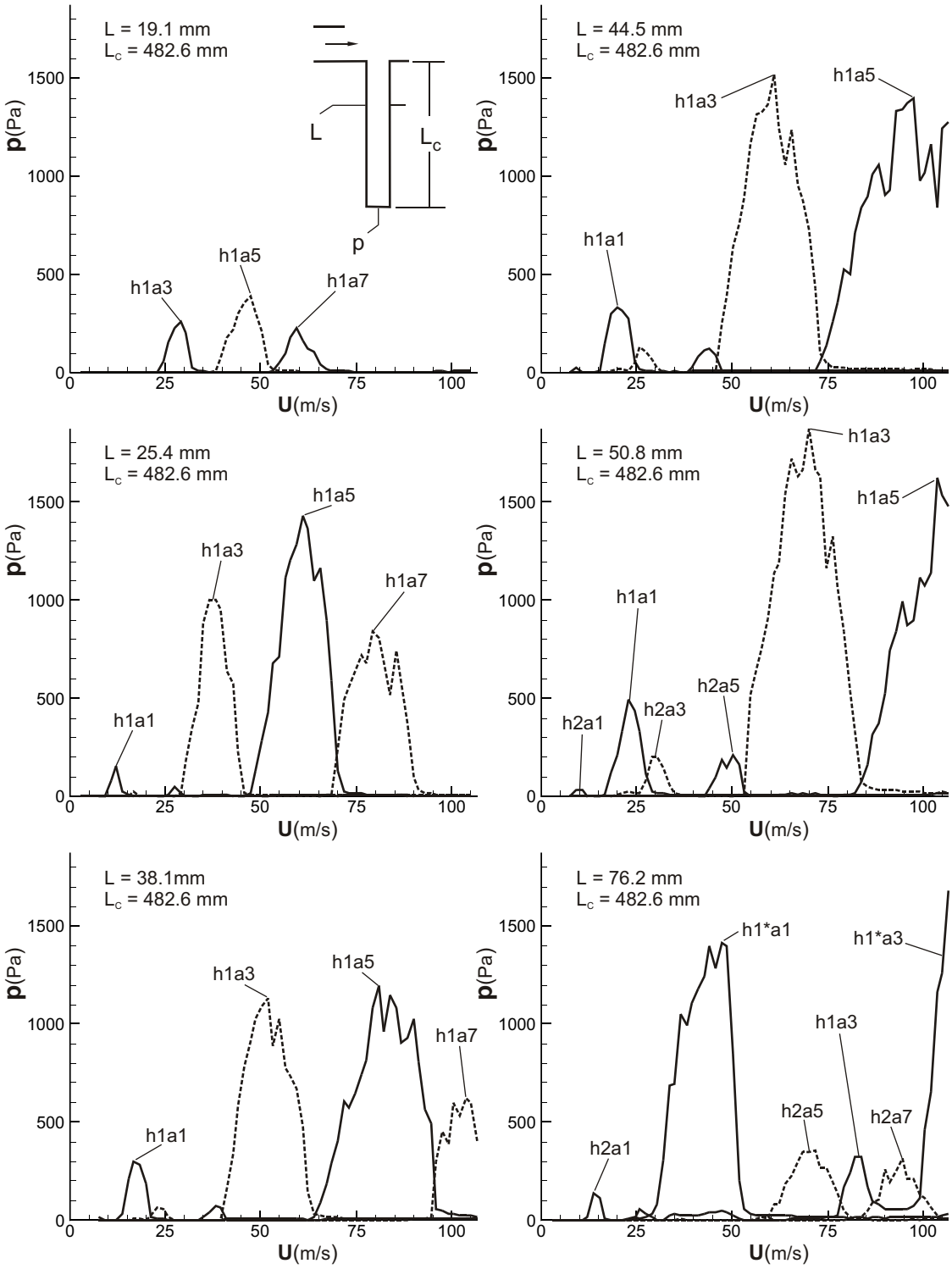

Figure 4: Variation of pressure amplitude *p* at the end of the deep cavity with inflow velocity *U* for the first *h1* and the second *h2* hydrodynamic modes and the first through the seventh acoustic modes *a1, a3, a5* and *a7*. Each plot corresponds to a different value of streamwise length *L* of the cavity opening.

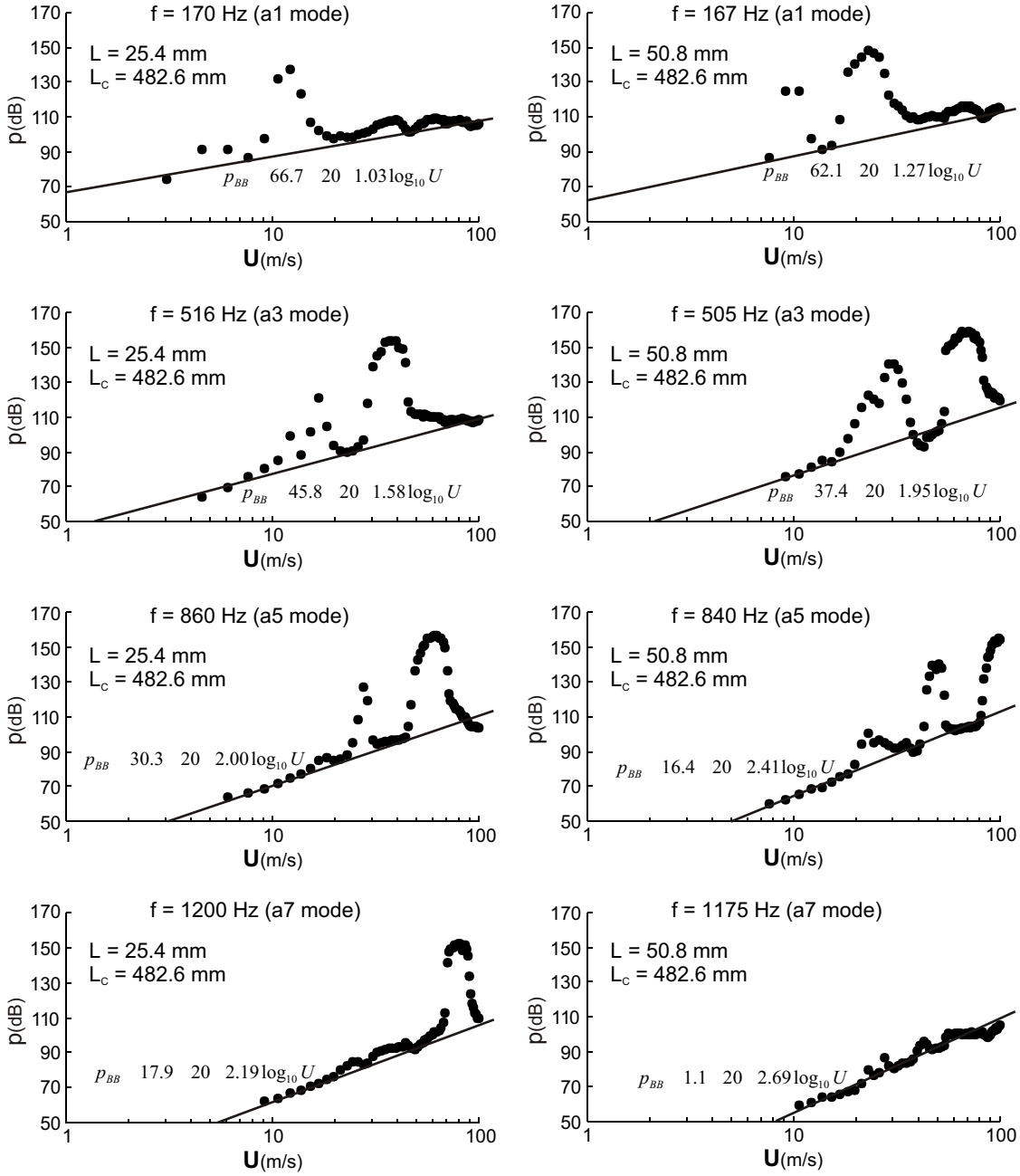

Figure 5: Variation of pressure amplitude p at the end of the deep cavity as a function of inflow velocity U relative to a reference line designated as p_{BB}, used for defining the strength of lock-on *SoL*.

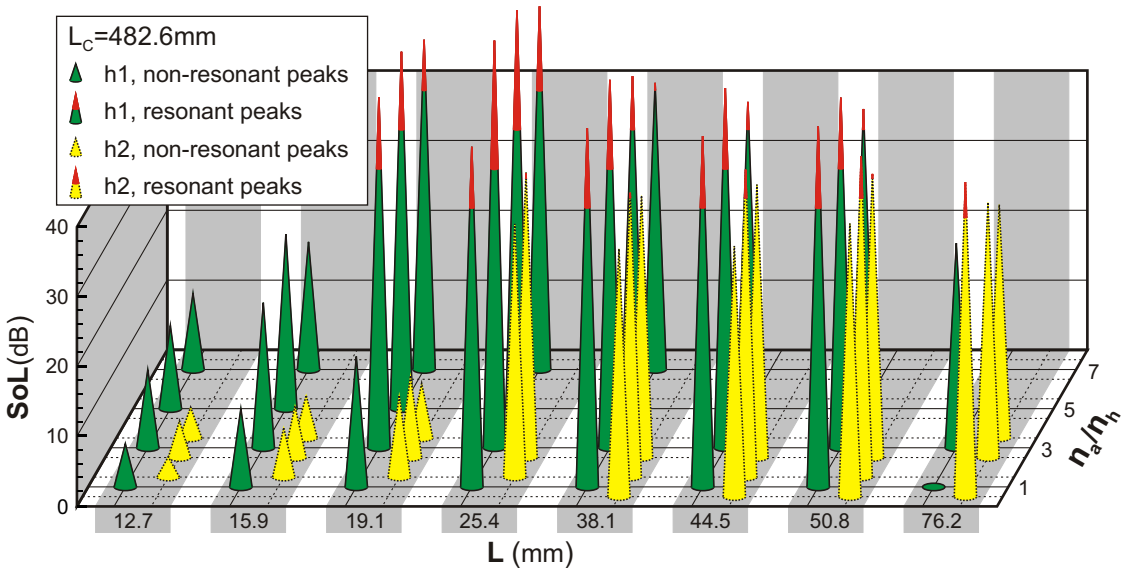

Figure 6: Representations of strength of lock-on *SoL* as a function of ratio of acoustic mode number n_a to hydrodynamic mode number n_h and the length L of the cavity opening. Symbols *h1* and *h2* correspond to the first and the second hydrodynamic modes (stages), with n_h = 1 and 2 respectively. Cavity depth corresponds to $L_C = 482.6$ mm.

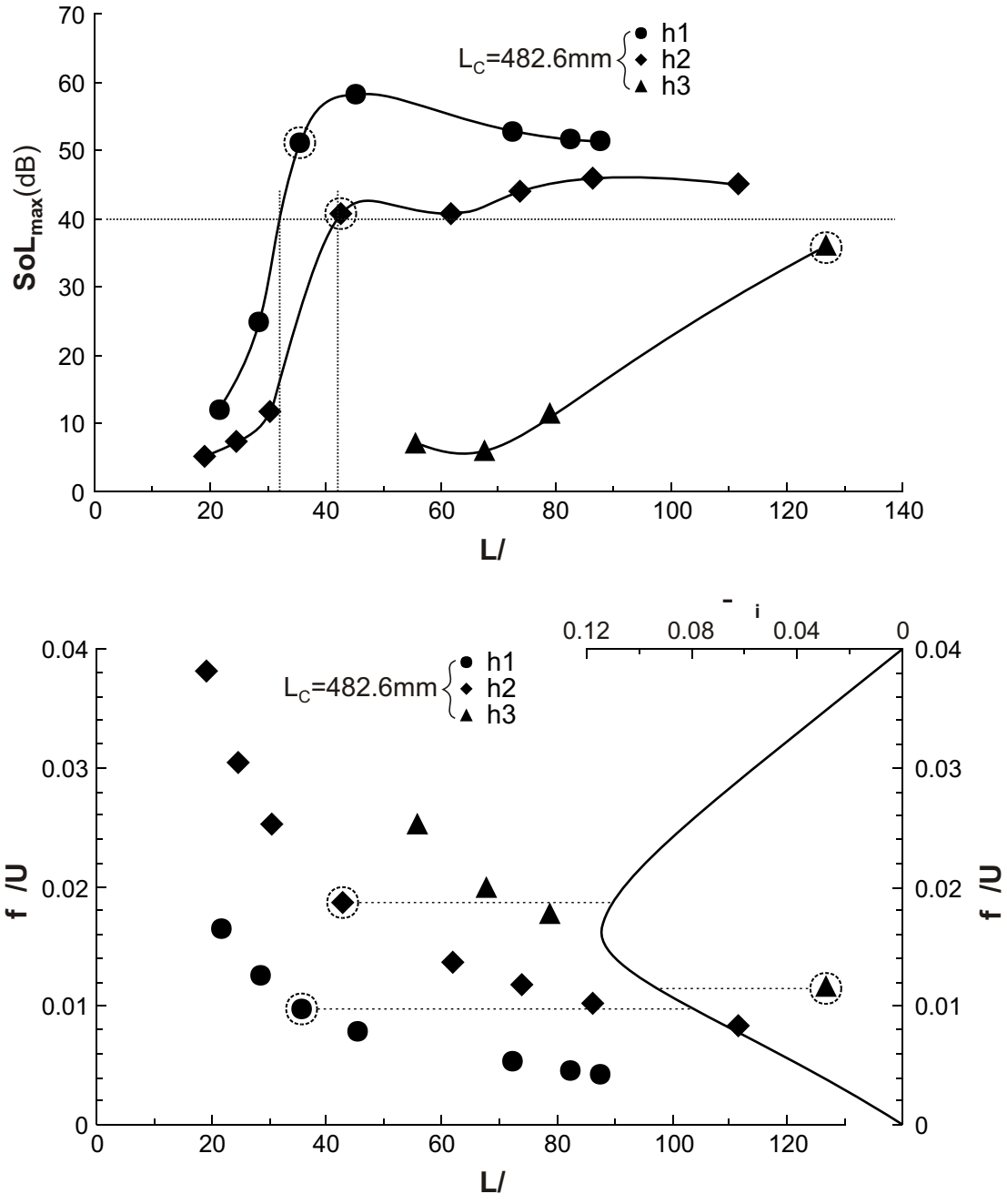

Figure 7: Variation of strength of lock-on SoL_{max} at the maximum deviation of pressure amplitude from the reference line as a function of streamwise length L of the cavity opening normalized by the momentum thickness of the inflow boundary layer (top plot), and variation of dimensionless frequency f/U as a function of $L/$ (bottom plot) in comparison with theoretically determined value of normalized amplification factor $-_i$ versus f/U (from Michalke, 1965). The cavity depth is of a fixed value $L_C = 482.6$ mm.

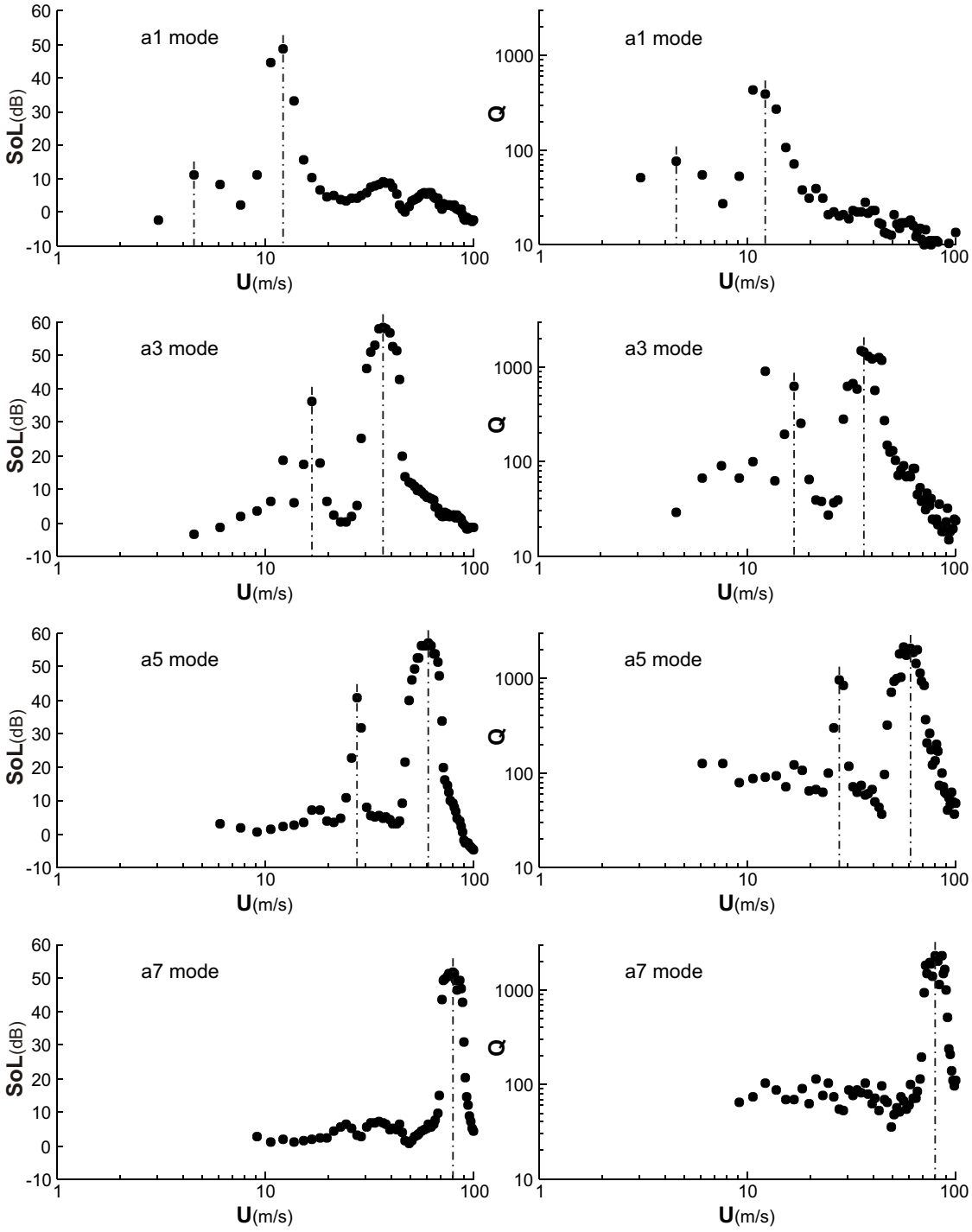

Figure 8: Strength of lock-on *SoL* as a function of inflow velocity U in comparison with corresponding values of quality factor Q as a function of inflow velocity U for the first through the seventh acoustic modes *a1* through *a7*. Streamwise cavity length $L = 25.4$ mm, cavity depth $L_C = 482.6$ mm.

L(mm)	Mode	U(m/s)	f(Hz)	p(Pa)	$p/0.5\rho U^2$	$p/\rho Uc$	SoL(dB)	Q	fL/U	$f\theta/U$
19.1	h1a3	29.0	519.0	255.2	0.503	0.0212	50.2	1400	0.341	0.0105
	h1a5	47.2	864.0	387.1	0.287	0.0197	51.1	2000	0.348	0.0098
	h1a7	59.4	1201.0	227.9	0.107	0.0092	47.2	2600	0.385	0.0103
25.4	h1a1	12.2	171.5	150.2	1.670	0.0296	48.7	390	0.357	0.0098
	h1a3	36.6	515.5	1004.9	1.242	0.0661	58.3	1400	0.358	0.0079
	h1a5	61.0	860.5	1429.2	0.636	0.0564	57.0	2100	0.359	0.0072
	h1a7	79.2	1198.5	838.8	0.221	0.0255	52.0	2300	0.384	0.0073
50.8	h1a1	22.9	167.5	496.6	1.571	0.0523	51.6	480	0.372	0.0045
	h1a3	70.1	504.0	1876.0	0.631	0.0644	50.1	1300	0.365	0.0035
	h1a5	103.6	835.0	1628.6	0.251	0.0378	42.9	1800	0.409	0.0037
	h2a1	9.1	166.5	35.7	0.705	0.0094	39.1	290	0.925	0.0136
	h2a3	29.0	505.0	202.0	0.398	0.0168	45.9	1000	0.886	0.0102
	h2a5	50.3	845.5	211.1	0.138	0.0101	40.6	1300	0.854	0.0089
76.2	h1*a1	47.2	168.0	1416.8	1.049	0.0722	48.9	330	0.271	0.0019
	h1a3	83.8	493.5	326.4	0.077	0.0094	29.3	670	0.449	0.0028
	h2a1	13.7	165.5	140.3	1.233	0.0246	45.0	440	0.919	0.0083
	h2a5	71.6	838.5	359.3	0.116	0.0121	36.5	830	0.892	0.0058
	h2a7	94.5	1165.5	313.6	0.058	0.0080	33.4	1100	0.940	0.0057

Table 1: Modes and parameters corresponding to the plots of Figure 4. Mode *h1a1* represents the coincidence of the first hydrodynamic mode (first stage) *h1* of oscillation of the shear layer and the first acoustic mode *a1* of the deep cavity. A similar designation holds for other hydrodynamic and acoustic modes. For each of these combinations, raw and dimensionless values of frequency *f* and amplitude *p* of each respective spectral peak are tabulated. In addition, the strength of lock-on *SoL* is given.